AD-A111 570 GEORGIA INST OF TECH ATLANTA SCHOOL OF ELECTRICAL EN--ETC F/G 20/6
SPACE/FREQUENCY CONVERSIONS IN IMAGE PROCESSING AND TRANSMISSIO--ETC(U)
NOV 81 W T RHODES AFOSR-78-3720

UNCLASSIFIED AFOSR-TR-81-0899 NL

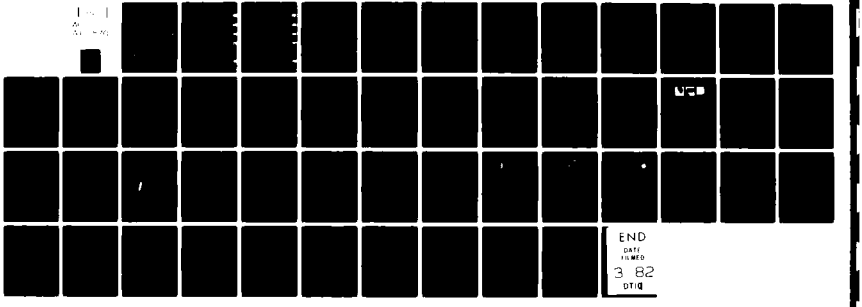

END
DATE FILMED
3 82
DTIC

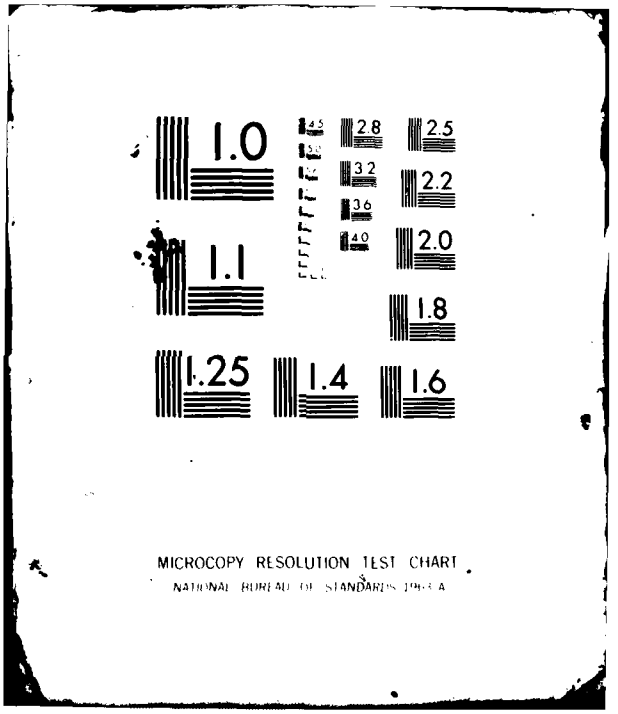
1.0
1.1
1.25
1.4
1.6
2.8
3.2
3.6
4.0
2.5
2.2
2.0
1.8
MICROCOPY RESOLUTION TEST CHART
NATIONAL BUREAU OF STANDARDS 1963-A

12

SPACE/FREQUENCY CONVERSIONS IN IMAGE PROCESSING AND TRANSMISSION

FINAL TECHNICAL REPORT ON

AFOSR [redacted] 78-3720

30 SEPT 78 - 29 SEPT 81

November 1981

William T. Rhodes
Georgia Institute of Technology
School of Electrical Engineering
Atlanta, Georgia 30332

Prepared for AFOSR/NE, Bldg. 410, Bolling AFB, D.C. 20332

UNCLASSIFIED

SECURITY CLASSIFICATION OF THIS PAGE (When Data Entered)

REPORT DOCUMENTATION PAGE	READ INSTRUCTIONS BEFORE COMPLETING FORM
REPORT NUMBER: AFOSR-TR- 81-0899	2. GOVT ACCESSION NO. / 3. RECIPIENT'S CATALOG NUMBER
SPACE/FREQUENCY CONVERSIONS IN IMAGE PROCESSING AND TRANSMISSION	5. TYPE OF REPORT & PERIOD COVERED: FINAL TECHNICAL REPORT 30 Sept 78 - 29 Sept 81
	6. PERFORMING ORG. REPORT NUMBER
7. AUTHOR(s): W. T. Rhodes	8. CONTRACT OR GRANT NUMBER(s): AFOSR 78-3720
9. PERFORMING ORGANIZATION NAME AND ADDRESS: Georgia Institute of Technology, School of Electrical Engineering, Atlanta, Georgia 30332	10. PROGRAM ELEMENT, PROJECT, TASK AREA & WORK UNIT NUMBERS: 61102F, 2305/B2
11. CONTROLLING OFFICE NAME AND ADDRESS: AFOSR/NE, Building 410, Bolling AFB, D.C. 20332	12. REPORT DATE: November 1981
	13. NUMBER OF PAGES: 50 incl. attachments
14. MONITORING AGENCY NAME & ADDRESS(if different from Controlling Office)	15. SECURITY CLASS. (of this report): UNCLASSIFIED
	15a. DECLASSIFICATION/DOWNGRADING SCHEDULE

16. DISTRIBUTION STATEMENT (of this Report)

Approved for public release; distribution unlimited.

17. DISTRIBUTION STATEMENT (of the abstract entered in Block 20, if different from Report)

18. SUPPLEMENTARY NOTES

19. KEY WORDS (Continue on reverse side if necessary and identify by block number)

Image Processing
Acoustooptic Processors
Frequency-Division Multiplex
Time-Integration Optical Processing
Optical Signal Processing

20. ABSTRACT (Continue on reverse side if necessary and identify by block number)

This research program centers on the investigation of a new optical/electronic method for highspeed convolution and correlation of two-dimensional imagery. The method, based on frequency-division multiplexing of image samples, is suited to implementation with wideband acoustooptic devices. During the report period the following has been accomplished:

1. Development of a time-integration method for obtaining

DD FORM 1 JAN 73 1473

UNCLASSIFIED

SECURITY CLASSIFICATION OF THIS PAGE (When Data Entered)

20 cont.

image output,

2. Development of methods for production of improved encoding/decoding local oscillator distributions,
3. Development of a general Fourier transform scanning hybrid image processor concept,
4. Development of important analogies between space-frequency conversion image processing, time-integration folded spectrum analysis, and Fourier transform holography,
5. Development of a joint-transform method for space-frequency conversion image processing,
6. Development of a significant method for increasing dynamic range in time-integration optical processing.
7. Development of a technique for reducing electronic system dynamic range requirements for space-frequency conversion image processing.
8. Devised methods for overcoming nonlinear phase response characteristics of acoustooptic cells in processing systems.
9. Development of a method for using common-band acousto-optic cells in time-integration folded spectrum analysis.
10. Devised a method for overcoming the need for wideband four-quadrant electronic multipliers in space-frequency conversion processing.
11. Developed a novel holographic beam combiner scheme that facilitates production of straight sinusoidal fringe patterns.

These developments enhance greatly the prospects that the space-frequency conversion scheme can be satisfactorily implemented in a wideband image processing system.

ABSTRACT

This research program centers on the investigation of a new optical/electronic method for highspeed convolution and correlation of two-dimensional imagery. The method, based on frequency-division multiplexing of image samples, is suited to implementation with wideband acoustooptic devices. During the report period the following has been accomplished:

1. Development of a time-integration method for obtaining image output.
2. Development of methods for production of improved encoding-decoding local oscillator distributions.
3. Development of a general Fourier transform scanning hybrid image processor concept.
4. Development of important analogies between space-frequency conversion image processing, time-integration folded spectrum analysis, and Fourier transform holography.
5. Development of a joint-transform method for space-frequency conversion image processing.
6. Development of a significant method for increasing dynamic range in time-integration optical processing.
7. Development of a technique for reducing electronic system dynamic range requirements for space-frequency conversion image processing
8. Devised methods for overcoming nonlinear phase response characteristics of acoustooptic cells in processing systems.
9. Development of a method for using common-band acoustooptic cells in time-integration folded spectrum analysis.
10. Devised a method for overcoming the need for wideband four-quadrant electronic multipliers in space-frequency conversion processing.
11. Developed a novel holographic beam combiner scheme that facilitates production of straight sinusoidal fringe patterns.

These developments enhance greatly the prospects that the space-frequency conversion scheme can be satisfactorily implemented in a wideband image processing system.

SUMMARY OF RESULTS AND THEIR SIGNIFICANCE

This research program has centered on the investigation of a new method for highspeed linear space invariant processing--spatial correlation or convolution--of 2-D imagery. The method is based on a frequency-division multiplex representation of a sampled image, where each spatial sample is represented by a separate temporal frequency carrier whose amplitude and phase are governed by the amplitude and phase of the sample. The processing method is suited to implementation using wideband acoustooptic devices. Major objectives of the research have been (1) a thorough conceptual and analytical understanding of the method, and (2) sufficient experimental experience to provide guidance for possible later developmental efforts by others.

Many of the basic concepts of the method are presented in Ref. [1], a copy of which is attached. Additional detail is presented in Refs. [2], currently in preparation, [5], and [12]. In the following paragraphs we delineate important results of the research program and their significance.

Conceptual and Analytical Investigations:

Development of a time-integration method for producing image output: When this research was proposed it appeared that output of the processed image would require the use of a 2-D spatial light modulator to serve as an interface between the electrical signal representation of the output image and the image itself [3]. In one of the most significant developments of this program we have showed how acoustooptic techniques under development for real-time folded spectrum analysis [4] can be employed for displaying output imagery in real time [1]. This development should allow an increase in image processing rate by roughly two orders of magnitude, up from TV frame rates to approximately 100 times that rate.

Development of methods for production of improved encoding-decoding local oscillator distribution: The encoding, or conversion, of a 2-D input image distribution to a frequency-division multiplex signal and the corresponding output conversion back to a spatial distribution require a 2-D array of light spots that vary in intensity sinusoidally with time, each spot varying at a different temporal frequency. Through the development of suitable mathematical models, we have been able to specify several modifications of existing techniques that allow the production of such "local oscillator" distributions with improved characteristics [5]. The main feature of these modifications is a sharpening of the encoding light spots and an attendant reduction in crosstalk between multiplexed signal components.

Development of Fourier transform scanning processor concept: In the course of looking for an experimentally simpler way of testing the basic space-to-frequency conversion processing concepts, we discovered a broad new class of real-time image proces-

sing techniques [6], of which the space-to-frequency conversion scheme is a member. These techniques, referred to as Fourier transform scanning image processing techniques, rely on an encoding of the magnitude and phase of a given spatial frequency component of an image as the magnitude and phase of a temporal frequency carrier. As the spatial frequency is scanned, a complex modulation of the carrier results. Electronic processing of the carrier produces a modification of carrier magnitude and phase, which corresponds to multiplication of the image spatial frequency spectrum by a transfer function.

The scheme is very powerful and more flexible than the space-to-frequency conversion scheme (which corresponds to the special case of scanning spatial frequency space in a repeated falling raster format). The latter scheme is still quite important, however, because only it is capable of fully exploiting the large operational bandwidth of acoustooptic devices in image processing.

Development of analogies between space-frequency conversion image processing, time-integration folded spectrum analysis, and Fourier transform holography: One of the most important conceptual/analytical contributions of this research program has been the development of useful analogies between space-frequency conversion processing, space- and time-integration folded spectrum analysis, and Fourier transform holography. These analogies, discussed in Ref. [5], have helped us and others to understand the limitations and possible improvements of these schemes, particularly with respect to the signal-to-noise ratio of the processed outputs.

Development of a joint-transform method for space-frequency conversion image processing: One of the more widely used methods for performing spatial correlations with coherent optical systems is the so-called joint-transform method, wherein both distributions to be correlated are input to the system simultaneously and a square-law device effectively multiplies their spatial frequency transforms. We have shown how the joint-transform method can be implemented in a space-frequency conversion, time-integration implementation [2]. There are two major advantages of this method: (1) only a single optical system need be used for both input distributions--with proper design, this system can, in fact, be used for simultaneous output as well; and (2) the joint-transform approach facilitates essential synchronization of input and output operations.

Development of a method for increasing dynamic range in time-integration optical processing: One of the serious limitations of time-integration optical processing is the buildup of bias in the output plane during processing [7]. Poor dynamic range arises in such processing because each momentary contribution to the output of the optical processor carries with it its own bias; the time-integrated bias uses up a major fraction of the available dynamic range of the output plane detector. Exploiting the analogies with Fourier transform holography noted

above, we have described a scheme for reducing this output plane bias to an absolute minimum [8]. Computer simulations indicate that the method allows roughly an order of magnitude increase in processed image dynamic range for TV-format imagery [8]. The importance of the proposed technique extends well beyond the image processing work of this program, for it is applicable to real-time spectral analysis and other forms of signal processing as well.

The minimum bias scheme described in Ref. [8] requires that the electrical signal representing the processed image undergo a square-root operation. Such an operation cannot be performed accurately on wideband signals, and thus presented a serious bottleneck for rapid, large dynamic range processing. On close inspection, however, we have concluded that the square root operation, necessary to assure minimum-bias output plane distributions in the output plane with the proper Fourier magnitudes, is not essential so long as we do not require that the detected output distribution be a perfectly faithful representation of the processed image. In particular, a logarithmic operation, easily performed on wideband signals, is adequate for all but the most demanding application. For matched filtering operations and most image processing applications the resultant output will be little changed from the ideal. Details are provided in Ref. [9].

Reduction of electronic system dynamic range requirements: In the original proposal it was noted that the result of the space-to-frequency conversion was an electrical signal of the form

$$g(t) = \sum_{m=1}^{N} g_m(t)\cos[2\pi(f_o + m\Delta f)t].$$

This signal is periodic and attains a maximum whenever the argument of the cosine equals an integer multiple of 2π radians. The dynamic range requirements on the attendant electrical signal processing subsystems can be extreme, and we consequently examined a variety of schemes for reducing the dynamic range of the converter output.

It was ultimately the development of the Fourier scanning image processor concept noted above that led to a solution. In particular, it can be viewed as the periodic encoding of the zero spatial frequency component of the input image that leads to the periodic maximum value of g(t). The solution to the problem is simple: through proper design of the optical system for encoding the input image it is possible to prevent the zero spatial frequency component from being encoded. Since this component generally conveys no useful information about the image to be processed, its exclusion does not adversely affect the resultant output image.

Experimental and Device Investigations:

Phase characteristics of acoustooptic cells: Early in our experimental work we determined that the phase response characteristics of acoustooptic cells would complicate system development immensely if different cells were used for image input and image output systems. The problem, basically, is that the phase of an acoustooptically diffracted light wave is not fixed to the phase of the rf input signal, but rather varies as a function of frequency in accord with the transfer characteristics of the particular cell. Two solutions were developed:

First, in discussions with Dr. R. Williamson of MIT Lincoln Laboratories, we determined that SAW chirp generators can be fabricated that precompensate the phase of an rf chirp as a function of frequency. If a properly precompensated chirp is input to the acoustooptic cell, the result is a diffracted light wave whose optical frequency increases linearly with time, as desired.

A second solution, the one we chose for our experimental investigations, requires that the same acoustooptic cells be used both for input of the two distributions to be convolved/correlated and for output of the resultant processed distribution. With such an approach it is possible to monitor the time-varying phase of the diffracted waves and employ coherent electronic signal processing techniques to compensate for any drift. This technique also allows for compensation of any phase drift introduced by aberrations and motion of components in the optical system.

Use of common-band acoustooptic cells: Early in our research it appeared that acoustooptic implementation of the scheme would require the use of two acoustooptic cells that operated in widely disperate frequency bands--one for a slow but wideband scan, the other for a rapid but smaller bandwidth scan. One of our minor achievements in this research was the discovery of a method for producing the required array of sinusoidally blinking light spots using a pair of acoustooptic cells that operate in essentially the same temporal frequency band. This method, described briefly in Ref. [5], allows implementation of the space-frequency processing scheme with potentially simpler electronics.

Highspeed multiplier problem: Another practical problem addressed during this research program was that of implementing the wideband signal multiplication necessary to produce the electrical signal representing the processed image. The operation requires a four-quadrant multiplier (i.e., one for which both input signals and the resultant output signal can be bipolar); unfortunately, four-quadrant multipliers with the required accuracy are limited in operational bandwidth to tens of megahertz [10]--inadequate for our purposes. We have solved this problem on paper by exploiting the bipolar signal multiplication capabilities of the acoustooptic devices themselves. The resultant scheme is similar in many respects to the triple-product acous-

tooptic processor investigated by Kellman et al with AFOSR support [11].

Holographic beam combiner: The experimental implementation we chose to investigate [6] required that we produce a moving sinusoidal fringe pattern incident on a pair of image transparencies. The spatial frequency of the fringes is changed by moving a pair of galvanometer-mounted mirrors in the optical system. It is essential that the fringes be straight: curved fringes correspond to a blurring of image information in spatial frequency space. In order to assure straightness of the fringes we employed a holographic beam combiner technique that is, to our knowledge, original. The basic idea involves making an interferogram of two nominally planar waves which is then used as a diffracting element to combine these two waves. When functioning as a combiner, the interferogram diffracts one of the incident waves and reconstructs a replica of the other. The diffracted wave then interferes perfectly with the original. If one or the other wave is tilted slightly at the combiner, the result is a pattern of highly regular fringes, as desired. The only requirement is that the phase aberrations of the original incident waves not be too great--say limited to 20 wavelengths or less. We believe that this scheme should facilitate the construction of a number of different kinds of interferometric optical signal processing systems. We are in the process of improving our holographic recording techniques and hope soon to publish the basic idea.

1. W. T. Rhodes, "Acoustooptic devices applied to image processing," in Real-Time Signal Processing II, F. Tao, ed. (Proc. SPIE, Vol. 180, 1979), pp. 145-149.

2. W. T. Rhodes, "Image processing via space-to-frequency conversions: concepts and theory," in preparation.

3. W. T. Rhodes, "Space-frequency conversions for image transmission and processing," Optics Letters, Vol. 3 (1978), pp. 24-25.

4. T. M. Turpin, "Time integrating optical processors," in Real-Time Signal Processing, F. Tao, ed. (Proc. SPIE, Vol. 154, 1978), pp. 196-203.

5. W. T. Rhodes, "The falling raster in optical signal processing," to be published in Transformations in Optical Signal Processing, W. Rhodes, J. Fienup, B. Saleh, eds. (SPIE, Bellingham, 1982; Vol. 2 in Advanced Institute Series). An excerpt from the manuscript for this paper is attached.

6. W. T. Rhodes, "Fourier transform scanning hybrid image processor," presented at the Eleventh Congress of the International Commission for Optics (ICO-11), Graz, Austria, September 1981.

7. P. Kellman, "Time integrating optical signal processing," Ph.D. dissertation, Stanford University, Stanford, CA, June 1979.

8. W. T. Rhodes, "Contrast in time-integration optical processing," in Proceedings of the 1980 International Optical Computing Conference, W. Rhodes, ed. (Proc. SPIE, Vol. 232, 1980), pp. 96-100.

9. W. T. Rhodes, "Bias reduction in time-integration optical processing," in preparation.

10. J. Leon, Doctoral Thesis Proposal, Georgia Institute of Technology, November 1981.

11. T. R. Bader. P. Kellman, and H. N. Shaver, "Time integrating optical signal processing," Final Technical Report on AFOSR Contract F49260-78-C-0102, July 1981.

12. W. T. Rhodes, Acousto-optic signal processing: convolution and correlation," Proc. IEEE, Vol. 69 (1981), pp. 65-79.

PUBLICATIONS AND PRESENTATIONS

Papers Published or in Press:

W. T. Rhodes, "Acoustooptic Devices Applied to Image Processing," in Real-Time Signal Processing, F. Tao, ed. (Proc. SPIE, Vol. 180, pp. 143-149, 1979).

W. T. Rhodes, "Contrast in Time-Integration Optical Processing," in Proceedings of the 1980 International Optical Computing Conference, W. T. Rhodes, ed. (Proc. SPIE, Vol. 232, 1980), pp. 96-100.

W. T. Rhodes, "Acousto-optic Signal Processing: Convolution and Correlation," Proceedings of the IEEE, Vol. 69, pp. 65-79 (1981).

W. T. Rhodes, "The Falling Raster in Optical Signal Processing," to be published in Transformations in Optical Signal Processing, W. T. Rhodes, J. R. Fienup, B.E.A. Saleh, eds. (SPIE Press, Bellingham, Wash.; Vol. 2 in Advanced Institute Series, 1982).

Papers in Preparation:

W. T. Rhodes, "Image Processing via Space-to-Frequency Conversions: Concepts and Theory."

W T. Rhodes, "Bias Reduction in Time-Integration Optical Processing."

Presentations:

W. T. Rhodes, "Acoustooptic Techniques in Space/Frequency Conversion Image Processing," SPSE Symposium on Optical Data Display, Processing, and Storage; Orlando, Florida, January 1979 (invited).

W. T. Rhodes, "Acoustooptic Devices Applied to Image Processing," 1979 SPIE-East Symposium, Washington, D.C., April 1979.

W. T. Rhodes, "Image Correlation Using Space-to-Frequency Conversions," 1979 Annual Meeting of the Optical Society of America, Rochester, NY, October 1979.

W. T. Rhodes, "Optical Heterodyne Systems in Real-Time Image Processing," LASERS '79 Conference, Orlando, December 1979 (invited).

W. T. Rhodes, "An Overview of Time-Integration Optical Processing," 1980 Gordon Research Conference on Holograpy and Optical Information Processing, Ventura, June 1980 (invited).

W. T. Rhodes, "Fourier Transform Scanning Image Processor," Information Systems Laboratory, Stanford University, February 1980 (invited).

W. T. Rhodes, "Contrast in Time-Integration Optical Processing," 1980 International Optical Computing Conference, Washington, D.C., April 1980 (invited).

W. T. Rhodes, "Transformations in Optical Signal Processing," Applied Optics Division, Naval Research Laboratory, Washington, D.C., October 1981 (invited).

W. T. Rhodes, "The Falling Raster in Optical Signal Processing," SPIE Advanced Institute on Transformations in Optical Signal Processing, Seattle, February 1981 (invited).

W. T. Rhodes, "Fourier Scanning Hybrid Image Processor," Eleventh Congress of the International Commission for Optics (ICO-11), Graz, Austria, September 1981.

LIST OF PERSONNEL INVOLVED IN RESEARCH

Faculty:

Dr. W. T. Rhodes, Professor, Principal Investigator
Dr. J. M. Florence, Research Associate
Dr. D. M. Hertling, Assistant Professor

Graduate Students:

R. Blum
K. Huther
J. Robinson
J. Selikoff
L. Shoun
C. Gliniak
R. Stroud (Ph.D. candidate)
J. Mait (Ph.D. candidate)

PROJECT-RELATED INTERACTIONS

January 1979, visited Dr. E. Young with the acoustooptics group at Harris Corp. in Melbourne, FL, to discuss acoustooptic signal processing and 2-D time-integration processing in particular. Additional discussions on grant-related topics with J. Boyde, L. Ralston.

April 1979, discussions at SPIE-East meeting in Washington, D.C., with Dr. John Neff of AFOSR, D. Hecht and P. Guilfoyle of ITEK, and C. Tsai of Carnegie-Mellon University.

April 1979, met with D. Stillwell of NRL and P. Kellman of ESL to discuss optical signal processing and get update on Dr. Kellman's AFOSR-sponsored research, which is complementary to this program.

May 1979, at two-day seminar on Optical Processing Systems sponsored by SPIE in Huntsville, Alabama, discussions with Drs. P. Kellman and T. Bader of ESL and J. Cohen of NSA on time integration optical processing. Additional related discussions with P. Guilfoyle of ITEK and R. Markevitch of Ampex Corporation.

June 1979, discussions with Drs. A. Sawchuk, T. Strand at USC Image Processing Institute regarding our respective AFOSR-supported research programs.

June 1979, met with P. Guilfoyle and D. Hecht of ITEK Corporation to discuss time-integration optical processing and acoustooptic device characteristics.

June 1979, met with Drs. P. Kellman and T. Bader at ESL, Inc., to discuss our respective complementary efforts with AFOSR support.

June 1979, discussed AFOSR project with Prof. J. W. Goodman at Stanford.

June 1979, met half day with H. Brown and L. Weiner of Ampex Corporation to discuss AFOSR research and related work.

October 1979, discussions on application of time-integration optical processing methods to DOD problems with Dr. Eugene Church of the Frankford Arsenal.

February 1980, presentation on work for Prof. J. W. Goodman and his students at Stanford University; additional discussions with Dr. Goodman and J. Erickson of Probe Systems regarding acousto-optic processing of imagery.

April 1980, at 1980 International Optical Computing Conference, discussions with Dr. John Neff of AFOSR and with Drs. Peter Kellman and Todd Bader of ESL regarding AFOSR researh projects.

May 1980, at ARO-sponsored workshop on Future Directions of Optical Information Processing at Texas Tech University. Technical discussions with Dr. John Neff (AFOSR), Dr. Bobby Guenther (ARO), and Mr. Harper Whitehouse (NOSC) regarding optical signal processing research activities in DOD.

May 1980, visit to U.S. Army Engineers Topographic Laboratory for discussions with Dr. Robert Leighty, including idea of using space-frequency conversions scheme in processing aerial photographic images.

June 1980, at Gordon Research Conference, technical discussions on AFOSR work with Dr. Todd Bader of ESL, Dr. John Neff of AFOSR, Dr. David Hecht of Itek Applied Technology Division, and Dr. Norman Berg of Harry Diamond Laboratory, generally centering on 2-D acoustooptic signal processing.

October 1980, interaction with Drs. J. Blodgett and H. Szu at Naval Research Laboratory.

December 1980, discussions with A. Tarasevich at Lockheed Electronics Company regarding multi-transducer acoustooptic devices for time- and space-integration optical processing.

February 1981, at SPIE Advanced Institute on Transformations in Optical Signal Processing, lengthy discussions with T. Turpin of NSA on the generation of 2-D local oscillator distributions for space-to-frequency conversions.

March 1981, during 2-D Signal Processing Symposium at Naval Research Laboratory, project-related interaction with P. Denzil Stilwell of NRL, Dr. John Neff of AFOSR, Peter Guilfoyle of Itek, Dr. Todd Bader of ESL, and Dr. Theo Kooij of DARPA.

March 1981, project-related interaction at Georgia Tech with Harper Whitehouse of the Naval Ocean Systems Center, Dr. John Neff of AFOSR (visiting for program review), and Prof. David Casasent of Carnegie-Mellon University.

May 1981, at Woods Hole Symposium, project-related interaction with P. Denzil Stilwell of Naval Research Laboratory and Dr. Theo Kooij of DARPA.

August 1981, visit to Applied Optics Laboratory at University of Erlangen in WEst Germany to discuss current research efforts with Prof. A. W. Lohmann; visit to Applied Physics Laboratory at

University of Heidelberg for discussions with Dr. F. Merkle.

ATTACHMENTS

1. Reprint of "Acoustooptic Devices Applied to Image Processing," by W. T. Rhodes, published in Real-Time Signal Processing II, F. Tao, ed. (Proc. SPIE, Vol. 180, 1979), pp. 143-149.

2. Reprint of "Contrast in Time-Integration Optical Processing," by W. T. Rhodes, published in Proceedings of the 1980 International Optical Computing Conference (Proc. SPIE, Vol. 232, 1980), pp. 96-100.

3. Reprint of "Acousto-Optic Signal Processing," by W. T. Rhodes, published in Proc. IEEE, Vol. 69 (1981), pp. 65-79.

4. Excerpts of "The Falling Raster in Optical signal Processing," to be published in Transformations in Optical Signal Processing, W. Rhodes, J. Fienup, and B. Saleh, eds. (SPIE, Bellingham, 1982; Vol. 2 in Advanced Institute Series).

Acousto-optic devices applied to image processing

William T. Rhodes
Georgia Institute of Technology
School of Electrical Engineering
Atlanta, Georgia 30332

Abstract

Two recently reported optical processing concepts can be exploited for realtime linear shift-invariant processing of 2-D imagery with acoustooptic devices: (1) space coordinate-to-temporal frequency conversion, and (2) time-integration spectral analysis. A pair of crossed acoustooptic cells, driven by periodic chirp waveforms, can be used for both operations. State-of-the-art acoustooptic devices appear suitable for gigahertz rate processing of images with spacebandwidth products approaching 10^4.

Introduction

Acoustooptic (AO) devices are applied regularly to the analysis and processing of 1-D signal waveforms because they allow realtime conversion of a time waveform into a corresponding light wave amplitude distribution [1]. They have been mostly disregarded for image processing applications (except as scanners and modulators) because of their inherently one-dimensional nature. Although a pair of AO devices might be crossed to produce a limited class (e.g., separable in cartesian coordinates) of light wave distributions, they cannot play the needed role of a general, electrically addressed 2-D spatial light modulator. There is, nonetheless, a way to exploit the attractive features of AO technology--wideband operation, no moving parts--in the highspeed processing of arbitrary 2-D imagery. The necessary keys to this exploitation are a space coordinate-to-temporal frequency mapping or conversion we recently reported [2] and a new class of AO spectral analysis operations recently described by Kellman and by Turpin [3,4].

Our overall goal is a hybrid optical-electronic system with the capabilities suggested by Fig. 1. In this figure, g(x,y;t) is a time varying input image, a function of spatial coordinates x,y, and of time t. The desired input-output relationship for the system is given either by a spatial convolution,

$$f(x,y;t) = g(x,y;t)*h(x,y;t) = \int_{-\infty}^{\infty}\int g(u,v;t)h(x-u,y-v;t)\,du\,dv, \tag{1}$$

or by a spatial cross correlation,

$$f(x,y;t) = g(x,y;t)\star h(x,y;t) = \int_{-\infty}^{\infty}\int g(u,v;t)h^*(x-u,y-v;t)\,du\,dv. \tag{2}$$

where we have allowed for the case of complex valued distributions by including a complex conjugation in the second integral. In order to describe the basic approach, we must consider four major concepts (the last two of which are closely related): (1) space coordinate-to-temporal frequency mapping; (2) spatial correlation and convolution via waveform multiplication; (3) AO input conversion; and (4) AO output conversion (display). In the following sections we describe these basic concepts and assess their implications for highspeed image processing.

Space Coordinate-to-Temporal Frequency Conversion

The first concept involves a reversible mapping or encoding (Fig. 2) of the input distribution, g(x,y;t), into a time waveform $g_f(t)$ via an ordered frequency-division multiplexing operation: the time function representing each element (pixel) of the time varying image modulates a different temporal frequency carrier. Both real-valued and complex-valued images can be encoded. Analytically, $g_f(t)$ is described by Eq. (3) below:

$$g_f(t) = \sum_{m=1}^{N^2} g_m(t)\cos[2\pi(f_o + m\Delta f)t + \theta_m(t)], \tag{3}$$

where

$$g_m(t) = |g(x_m,y_m;t)| \tag{4}$$

$$\theta_m(t) = \arg[g(x_m,y_m;t)]. \tag{5}$$

In Eqs. (4) and (5), $g(x_m,y_m;t)$ is the value of g(x,y;t) at the mth sample location in a regular NxN sampling array. As shown in Fig. 3, these samples are ordered in a left-to-right, top-to-bottom fashion. Equation (3) thus represents the following: The input, g(x,y;t), assumed to be of finite spatial bandwidth and extent, is

sampled spatially. By assumption, the distance between samples satisfies the Nyquist sampling condition. The magnitude and (if complex-valued) phase of the sample value at the mth sample location are given by $g_m(t)$ and $\vartheta_m(t)$. For each m, $g_m(t)$ and $\vartheta_m(t)$ then serve to modulate the magnitude and phase, respectively, of a cosine at frequency $f_m = f_o + m\Delta f$. The output of the space-to-frequency encoder, $g_f(t)$, which equals the sum of all such modulated carriers, thus represents the entire NxN image array.

So long as the temporal frequency bandwidth of each term in the summation is sufficiently small compared to Δf, the individual terms do not overlap in frequency content, and $g_f(t)$ is an unambiguous representation (through the sampling theorem) of g(x,y;t). Specifically, an inverse mapping is possible.

Figure 4 illustrates with the case of a 5x5 array of non-time varying image samples, for convenience assumed to be nonnegative-real and of integer value. The spectrum $G_f(f)$ is the Fourier transform of $g_f(t)$. If g(x,y;t) varies with time, the discrete spectral components shown broaden out into narrowband components (by assumption, non-overlapping).

In Ref. 1 we noted (as have others) that such a representation provides an alternative to conventional scanned signal representations for transmitting images. Our interest here is in how this mapping can be applied to highspeed image processing, as we discuss in the following section. Later, we shall return to the question of how to perform the space-to-frequency mapping.

Spatial Convolution and Correlation Via Waveform Multiplication

In Fig. 5 we show in diagram form a system suitable for real time convolution or correlation of a pair of input images or other spatial distributions represented by g(x,y;t) and h(x,y;t). In between the pair of space-to-frequency encoders at the left and the frequency-to-space decoder at the right--both of which will be described later--the system consists of conventional electronic subsystems: heterodyne converters, a waveform multiplier, and a bandpass filter. The heterodyne converters simply move the collection of modulated carriers representing g(x,y;t) and h(x,y;t) up or down in frequency as a group. Thus

$$g'_f(t) = \sum g_m(t)\cos[2\pi(f_o + f_1 + m\Delta f)t + \vartheta_m(t)], \tag{6}$$

where f_1 is the amount of frequency shift. Similarly for $h'_f(t)$ and $h_f(t)$.

The heart of the system is the multiplier. Multiplication of two time waveforms implies convolution of the corresponding spectra. But in this case, the spectra represent, on a sample-by-sample basis, the elements of the two spatial distributions to be convolved. It is a consequence of the particular ordered encoder mapping chosen that convolution of the two spectra correspnds to a convolution (or correlation, depending on system setup) of the corresponding 2-D spatial distributions g(x,y;t) and h(x,y;t).

It is easiest to see this by considering an example, in this case a convolution. Let the two arrays in Fig. 6 represent a pair of sampled image intensity distributions g(x,y) and h(x,y), assumed to be non-time varying. The actual image arrays are 3x3 in extent, but since convolution of two 3x3 arrays yields a 5x5 array, it is necessary to encode g(x,y) and h(x,y) in larger 5x5 arrays with zeros around the edge. The corresponding spectra $G_f(f)$ and $H_f(f)$ are also shown. Assuming the frequency offsets for the two signals to be sufficiently great, multiplication of $g_f(t)$ by $h_f(t)$ produces two groups of non-overlapping temporal frequency components, corresponding to sum and difference frequencies. The sum frequencies are shown in Fig. 7(a), obtained by convolving the distributions of Figs. 6(c) and 6(d). These components are isolated by the bandpass filter and heterodyne-converted down in frequency for decoding/display. The resultant 2-D output distribution, obtained according to the inverse of the mapping of Fig. 3, has sample values proportional to those shown in Fig. 7(b), the desired 2-D convolution. It is easily shown that the difference frequencies generated by the multiplication correspond to the cross correlation of g(x,y) with h(x,y). Thus a minor change in bandpass filter characteristics allows either g(x,y)*h(x,y) or g(x,y)•h(x,y) to be obtained as output.

Acoustooptic Input Conversion

The system employed for encoding an input 2-D distribution as a frequency-division multiplex signal waveform will depend in form on whether the input is a light intensity distribution or a complex wave amplitude distribution. We consider first the encoding of nonnegative real intensity distributions, then note modifications appropriate for complex valued amplitude distributions.

Assume that the input to be encoded, g(x,y;t), exists as the light intensity transmittance of a realtime spatial light modulator (SLM). (Since we are concerned only with the intensity transmittance of the SLM, surface quality requirements can be relaxed from those necessary for coherent optical processing.) The basis for the encoding operation is illustrated in Fig. 8, where we show the mth element of the SLM illuminated by a focused beam of light. This light beam is modulated sinusoidally in intensity at frequency $f_m = f_o + m\Delta f$, as appropriate for sample location (x_m,y_m). Since the light power transmitted by the SLM is proportional to $g(x_m,y_m;t)$, the output of the photodetector contains an a.c. term proportional to $g(x_m,y_m;t)$, where $\omega_m = 2\pi f_m$.

Obviously what is desired is an array of light beams, NxN in extent, with all beams incident on the SLM simultaneously and each blinking sinusoidally at a rate appropriate to the spatial element it illuminates.

Assuming the photodetector to be sufficiently large that all the light transmitted by the SLM is collected, the detector output will then contain a term proportional to $\int g_m(t)\cos[2\pi(f_o + m\Delta f)t + \theta_m(t)]$, as desired. For this case, $g_m(t) = g(x_m,y_m;t)$, and the phase angle $\theta_m(t)$ depends on the relative phase of the illuminating light spot variations.

A system for producing a single encoding spot at blink frequency f_m is shown in Fig. 9. Here an AO cell is driven by a sinusoid at frequency f_m. In the back focal plane of the lens the +1 diffraction order is brought to a focus at the mth cell of the SLM, where it mixes with light brought around by the beamsplitter/mirror combination. The interaction of light with sound in the AO device increases the optical frequency of the +1 diffraction order from the base laser frequency ($\sim 5\times10$ Hz) by an amount equal to f_m. Depending on the AO device used, f_m may range from several megahertz to several gigahertz. Using phasor representations [5] for the two mixing wave fields (and assuming equal amplitudes), we have for the light intensity at (x_m,y_m)

$$I(x_m,y_m) = \left| 1 + e^{j2\pi f_m t} \right|^2 = 2(1 + \cos 2\pi f_m t), \tag{7}$$

which is of the desired form.

Multiple spots of light, each blinking at a different frequency, can be produced by driving the AO cell simultaneously with a number of cosine waveforms, each at a different frequency. The diffraction angle--and therefore the location of the resultant spot in the encoding plane--will depend on the frequency of the particular waveform component, the distance of the spot from the optical axis being proportional to f_m. Specifically, driving the AO cell with signal $s(t)=\sum\cos[2\pi(f_o + m\Delta f)t]$ will produce a row of equally spaced light spots separated in blink frequency by Δf. High diffraction efficiency is not possible with such an input signal because of the inherent nonlinearities of the AO interaction. It is possible, however, to obtain a time varying wave intensity of the desired form at the sample locations by driving the cell with a periodic chirp waveform, where the frequency of the input sinusoid is ramped linearly with time in a repetitive manner [6]. Greater diffraction efficiency is possible under these circumstances. For pedagogical reasons we will assume that the driving signal consists of discrete sinusoids. In practice, however, the periodic chirp waveform is more likely to be used.

The system of Fig. 9 will produce a 1-D array of light spots if driven with the correct sum of sinusoidal signals. We need, however, a 2-D encoding array of light spots. The answer to this problem is to use a second AO cell operating at right angles to the first. The basic idea is illustrated in Fig. 10. In Fig. 10(a) we show a horizontally aligned AO cell driven by a sum of zero-phase cosines spaced by Δf in frequency. The light spots in the associated diffraction pattern, in the back focal plane of the lens, are separated in optical frequency by Δf. Figure 10(b) shows an orthogonally oriented cell driven at frequencies that are integer multiples of $N\Delta f$, where NxN is the size of the array to be encoded. As indicated, adjacent diffraction spots from this cell are separated in frequency by $N\Delta f$. If these two orthogonal cells are placed in close contact (or, in practice, imaged onto one another), their spatial transmittance functions multiply, with a resultant convolution of the associated diffraction patterns, as shown in Fig. 10(c). It is easily shown, by considering how the frequency shifts add on a spot-by-spot basis, that the encoding spots in the resulting 2-D array are separated by Δf in one direction and by $N\Delta f$ in the other. This is, of course, precisely what is desired for an NxN encoding array. In practice, an NxN array of frequency-shifted spots is selected to mix with a non-frequency shifted plane wave. The resultant array of intensity-modulated light spots then transilluminates the SLM, as described earlier.

With some modification, the basic scheme described above can be used to encode complex-valued spatial distributions [2,7]. For example, let $g(x,y;t)$ be the complex wave amplitude distribution in the Fourier transform plane of a coherent optical processor. If this distribution is mixed at a large area detector with the array of frequency-shifted encoding spots, the detector output signal will contain the desired signal $g_f(t)$ given in Eq. (3). Should $g(x,y;t)$ be the complex amplitude transmittance of a SLM, it can be encoded by transilluminating the SLM with the frequency shifted encoding array prior to mixing with the non-frequency shifted reference wave.

Several notes are in order. First of all, the finite length of the AO cell aperture will produce a spreading, or smearing, of the individual light spots. To the extent that the frequency shifted beams overlap spatially, their interference will produce light intensity fluctuations throughout the entire encoding region at low integer multiples of Δf and $N\Delta f$. Since these fluctuations are not specific to any one sample location, it is necessary to work with an array of light spots well removed from the optical axis of the transform lens. Under these circumstances the offset frequency f_o in Eq. (3) is sufficiently high that the desired frequency-division multiplex components of the detector output are separated in frequency from the nonspecific lower frequency terms.

A second point relates to the aspect ratio of typical AO devices. For reasons of power consumption and diffraction efficiency, the opto-acoustic interaction region for most AO cells is long and narrow. As a consequence, anamorphic lens systems of large differential magnification are required if one cell is to be imaged entirely onto another for generation of the 2-D encoding array.

The third point relates to the bandwidth required of the AO devices. In order to operate as suggested in Fig. 10, it is necessary that one cell operate in a frequency band N times higher than the other. If N is large, this necessitates the use of two substantially different devices, one operating, for example, in the

tens of megahertz range, the other operating in the gigahertz range. An attractive alternative is suggested in Fig. 11. If two cells, one driven at integer multiples of NΔf and the other at integer multiples of (N-1)Δf, are oriented approximately 45° to each other and placed in optical contact, the resultant diffraction pattern has the appearance shown at the right of Fig. 11. As shown, the separation in optical frequency of adjacent spots is Δf in one direction and NΔf in the other, as desired for the encoding. The important characteristic of this scheme is, of course, that the two cells operate in essentially the same frequency range. There is, however, some sacrifice in the size of the array that can be encoded.

Finally, we note that the dynamic range of the signal waveform $g_f(t)$ may be quite large if all the carriers of Eq. (3) are modulated with the same phase. This is of necessity the case when nonnegative-real (intensity) distributions are to be encoded for processing purposes. If simple image transmission (see Ref. 2) is the goal, the ϕ_m can be randomized to reduce the range of $g_f(t)$. If bipolar-real processing is the goal, it is possible to perform operations analogous to bipolar noncoherent spatial filtering [8] with reduced dynamic range. A description of these operations is beyond the scope of this paper.

Acoustooptic Output Conversion (Display)

Figure 12 illustrates a system suitable for the conversion of the processor output signal waveform $f_f(t)$ into the corresponding 2-D display $f(x,y;t)$. This display system is based on a 2-D time integration spectrum analysis scheme described by Turpin and by Kellman [2,3]. A modified spectrum analysis scheme proposed by Bader is also applicable [6]. In the system of Fig. 12, an NxN array of appropriately frequency-shifted spots (produced by a pair of AO cells, as described earlier) mixes in the output plane with a mutually coherent plane wave that is modulated in time by the signal $f_f(t)$. (The modulation, on a wave amplitude basis, can be accomplished using another acoustooptic cell driven by signal waveform $f(t)$.) At the mth sample location in the output plane, the display intensity is thus given by

$$I_{disp}(x_m,y_m;t) = \left| e^{j\omega_m t} + f_f(t) \right|^2, \tag{8}$$

where $\exp[j\omega_m t]$ is the phasor representation of the mth frequency-shifted light spot. If we substitute for $f_f(t)$ (using Eq. (3) with f for the magnitude and ϕ for the phase) and collect terms, we obtain

$$I_{disp}(x_m,y_m;t) = 1 + f_f^2(t) + 2\sum_{k=1}^{N^2} f(x_m,y_m;t)\cos[\omega_k t + \phi(x_m,y_m;t)]\cos\omega_m t. \tag{9}$$

The first and second terms correspond to a uniform bias across the entire display. The third term evaluates to $f(x_m,y_m;t)\cos\phi(x_m,y_m;t) = \mathrm{Re}\, f(x_m,y_m;t)$, with the result

$$I_{disp}(x_m,y_m;t) = \mathrm{Bias} + \mathrm{Re}\, f(x_m,y_m;t), \tag{10}$$

a low contrast version of the real part of the output distribution. If $f(x,y;t)$ is real valued, this is all that is sought. For complex-valued $f(x,y;t)$, the imaginary part is obtained by shifting the optical phase of one of the distributions by $\pi/2$ radians.

Implications for Highspeed Image Processing

The overall system of Fig. 9--encoders, processor, decoder--are all capable of operation at high speed for a variety of realtime image processing applications. Multiplier and filtering electronics for the processor with gigahertz bandwidths are well within state-of-the-art capability. The acoustooptic devices used for encoder and decoder can provide 1-D spacebandwidth products up to 1000 or more, for a total image size approaching 1000x1000. Operational bandwidths for wideband AO devices now exceed one gigahertz. It thus appears that gigahertz-rate processing of 1000x1000 element imagery should be achievable with state-of-the-art technology, corresponding to roughly 1000 2-D correlations per second. The actual rate at which $g(x,y)$ and $h(x,y)$ can change will be limited in many cases by the SLMs employed. In one important area of application, target acquisition and tracking, the input image may change relatively slowly, while the spatial impulse response $h(x,y;t)$ is varied rapidly in a pattern recognition search operation. Under these circumstances, $h_f(t)$ need not exist in 2-D spatial form. Rather, it can be stored in 1-D serial form and input at high speed directly into the multiplier.

We note in conclusion that an experimental program has been begun to demonstrate the concepts discussed above using AO technology. This work is being supported by a grant from the U.S. Air Force Office of Scientific Research. Funding for much of the conceptual development came from the U.S. Army Research Office.

References

1. Several papers in this proceedings provide up-to-date information on this subject.
2. W. T. Rhodes, "Space-frequency conversions for image transmission and processing," Optics Letters 3 (1978) 24-26.
3. T. M. Turpin, "Time integrating optical processors," in Real-Time Signal Processing, T. F. Tao, ed. (Proc. SPIE, Vol. 151, 1978), pp. 196-203.
4. P. Kellman, "Detector integration acousto-optic signal processing," in Proceedings of the 1978 International Optical Computing Conference (Digest of Papers) (IEEE Pub. 78CH1305-2C, 1978), pp. 91-95.
5. J. W. Goodman, Introduction to Fourier Optics (McGraw-Hill, 1968), Chapt. 3.
6. T. R. Bader, "Acoustooptic spectrum analysis: A high performance hybrid technique," to appear in Applied Optics.
7. W. T. Rhodes, "Image processing using space-to-temporal frequency conversion," in Optica Hoy y Mañana, Proceedings of the Eleventh Congress of the International Commission for Optics, Bescos et al., eds. (Instituto de Optica "Daza de Valdes," C.S.I.C., Sociedad Espanola de Optica, Madrid, 1978), pp. 261-264.
8. W. T. Rhodes, "Bipolar pointspread function synthesis by phase switching," Appl. Opt. 16 (1977) 265-267.

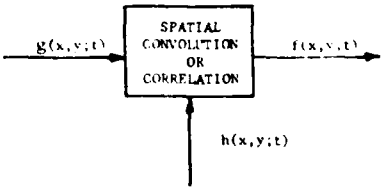

Fig. 1. Hybrid optical-electronic image processing system performs spatial convolution or correlation of two input distributions, each potentially time varying.

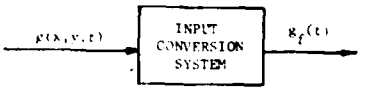

Fig. 2. Optical-electronic system encodes time-varying 2-D input distribution, g(x,y;t), as collection of modulated temporal frequency carriers.

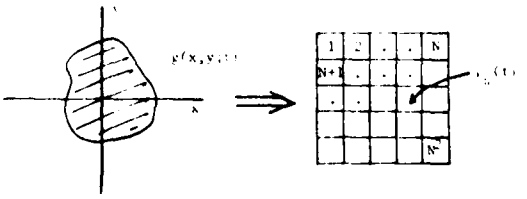

Fig. 3. N^2 temporal frequencies correspond to a left-to-right, top-to-bottom ordering of associated NxN array of spatial samples of image.

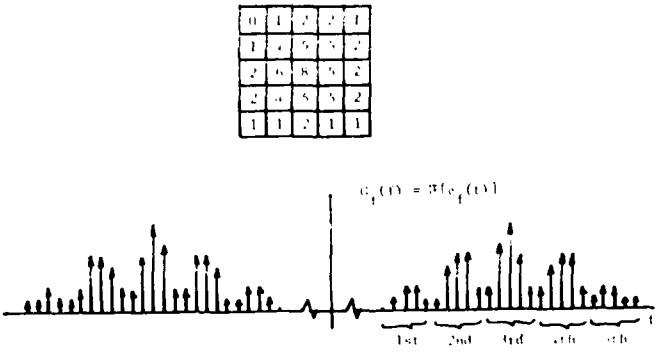

Fig. 4. Example: 5x5 image (intensity) sample array and spectrum of associated 1-D frequency-division multiplexed signal representation. Spectral components are grouped according to row number in image.

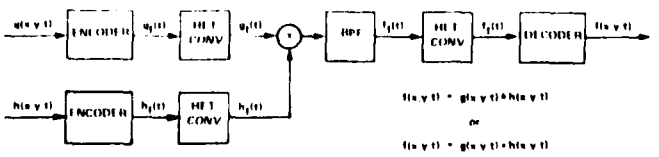

Fig. 5. System diagram for realtime convolver/correlator. BPF denotes bandpass filter, HET CONV denotes heterodyne converter.

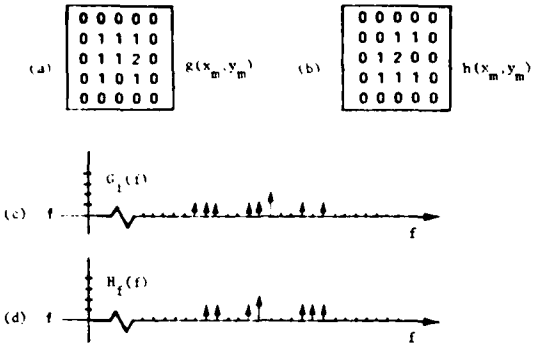

Fig. 6. Example of 2-D convolution with frequency coded signals. Inputs assumed to be nonnegative-real and with integer sample values. Only positive frequency components are shown.

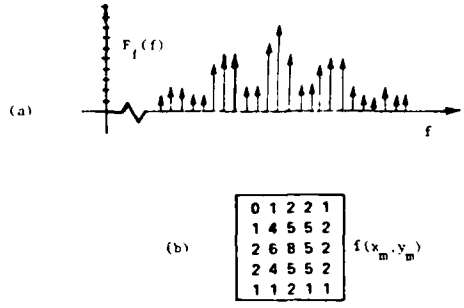

Fig. 7. Spectrum of system output (a), and associated decoded spatial distribution (b) resulting from convolution of two arrays in Fig. 6.

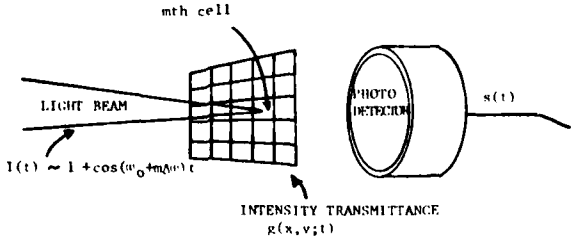

Fig. 8. Encoding single image sample with sinusoidally modulated light beam.

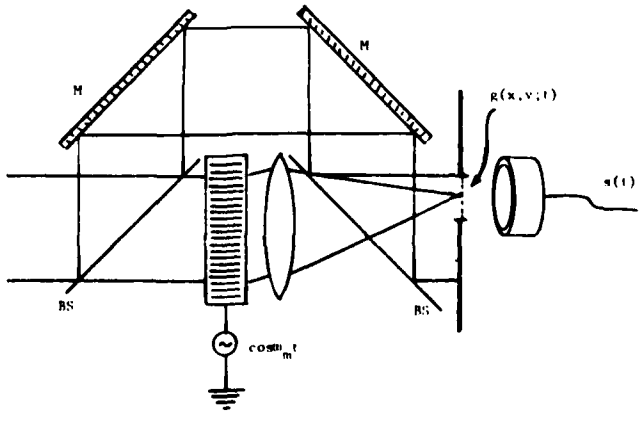

Fig. 9. Interferometer-based system with acoustooptic cell for FDM encoding spatial samples of input image. SLM is placed in encoding aperture, in front of large area detector.

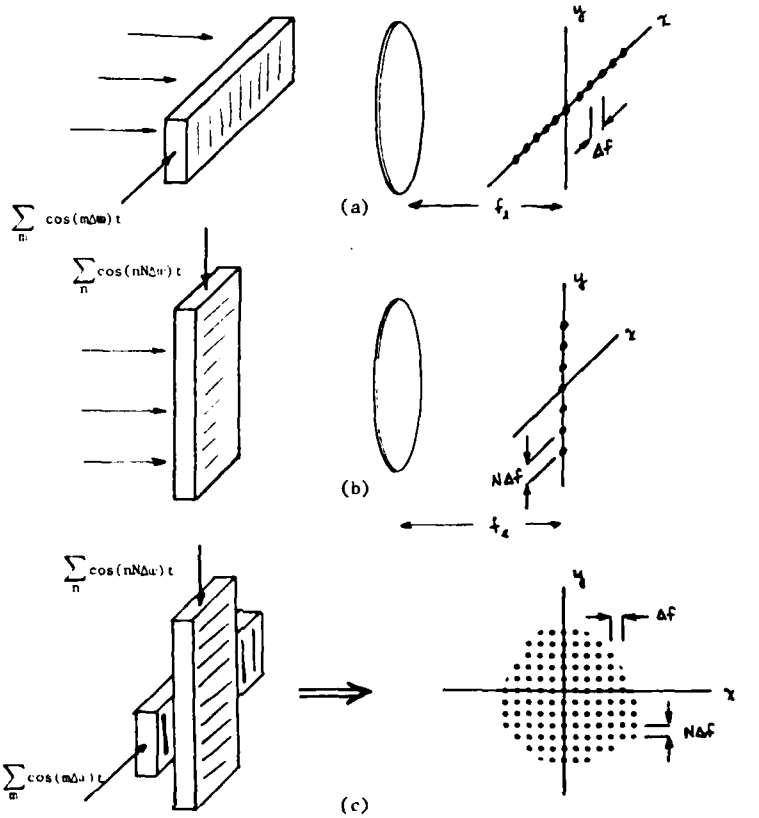

Fig. 10. Use of acoustooptic cells in generating array of frequency-shifted encoding light spots.

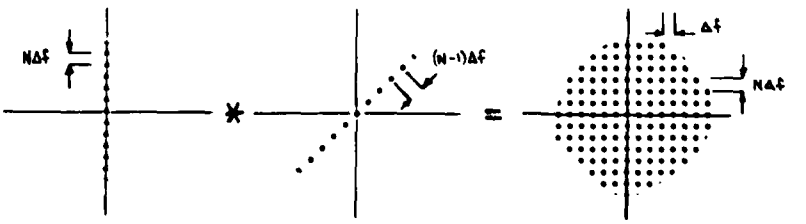

Fig. 11. Encoding array can be obtained with two acoustooptic cells operating in same frequency range if they are crossed at 45°.

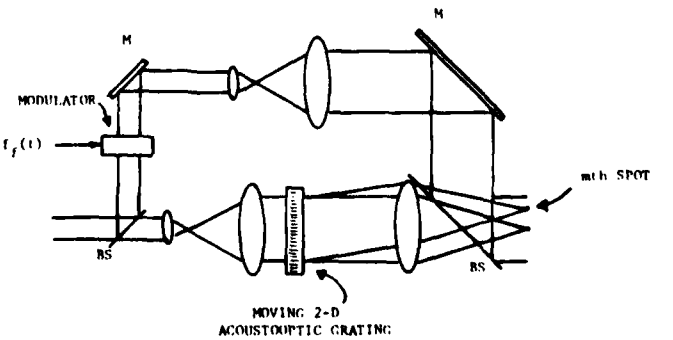

Fig. 12. Time integration spectrum analyzer for output conversion/display of processed image.

Contrast in time-integration optical processing

William T. Rhodes
Georgia Institute of Technology, School of Electrical Engineering, Atlanta, Georgia 30332

Abstract

The problem of bias buildup in time-integration image processing is assessed. Numerical studies are presented that compare the results of the usual approach to interferometric time-integration processing with a proposed minimum-bias approach. It is concluded that the latter approach yields outputs of dynamic range adequate for many practical image processing situations.

Introduction

Time-integration optical processing methods have been used for 1-D signal correlation, 1-D spectrum analysis, and ambiguity function processing [1-12]. Although many processing operations described in the literature are 1-D in nature, 2-D systems have been described for large time-bandwidth product spectral analysis of 1-D signals [4-6.8-11]. Our own interest lies in the application of time-integration methods to the processing of 2-D imagery. The reason, without going into detail [13-16], is that we have available to us a signal waveform $v_f(t)$, that represents as a function of time a scanned version of spatial frequency transform $F(u,v)$. In order to obtain the corresponding output image, $f(x,y)$, it is necessary to inverse Fourier transform $F(u,v)$. This can be done spatially if $F(u,v)$ is recorded as a hologram and Fourier transformed with a lens. It is more direct, however, if the spatial frequency components of $f(x,y)$ are added up sequentially in time - i.e., via time integration.

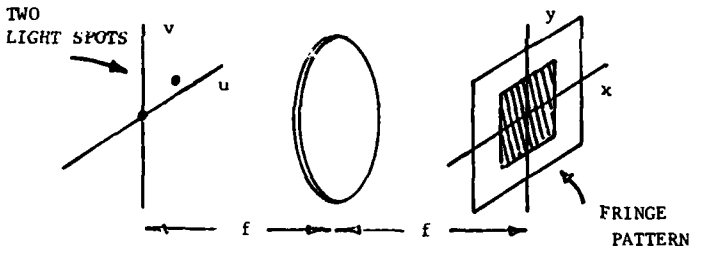

Fig. 1. Two coherent light spots producing fringe pattern

The basic idea is illustrated in Fig. 1. In the input plane are two mutually coherent light spots, one or both of which can be moved about and varied in magnitude and relative phase. The corresponding intensity distribution in the output plane is a sinusoidal fringe pattern whose spatial frequency is governed by the vector separation of the two light spots and whose contrast, magnitude, and phase are governed by the magnitudes and relative phase of the light spots. The essence of the time-integration image synthesis procedure is to build up a composite image distribution, fringe pattern by fringe pattern. This is basically a Fourier synthesis operation, each sinusoidal intensity fringe pattern corresponding to a Fourier component of the image distribution. A system that could be used in producing such a fringe pattern is illustrated in Fig. 2. The two light spots producing the fringe pattern are moved about for different vector spacings via two orthogonally driven galvanometer-mounted mirrors. Magnitude and phase of the two light spots are varied by the modulators.

A major problem with such an image synthesis operation is immediately evident: as every fringe pattern, or Fourier component, carries with it some bias, the superposition of a large number of components will generally result in a low constrast image. Should the signal-to-bias ratio be sufficiently low, available detectors (either film or electronic) will be incapable of recording the image with good signal-to-noise ratio.

In what follows, we consider two approaches to producing these fringe patterns and calculate numerically the results for typical imagery. We are then in a position to draw conclusions regarding the viability of time-integration schemes in image processing.

Constant Reference Synthesis

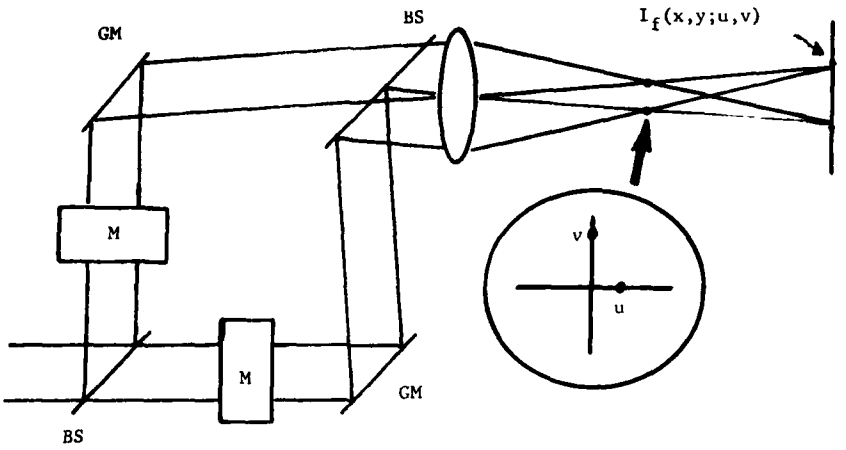

Fig. 2. System for producing sequence of fringe patterns.

Our objective with the system of Fig. 2 is to produce, sequentially in time, a sequence of sinusoidal intensity fringe patterns corresponding to real Fourier components of the form $|F(u,v)|\cos[2\pi(ux+vy) + \arg(F(u,v))]$. A straight-forward method of doing so is to keep the amplitude of one wave in the output plane of Fig. 2 equal to a constant, R_o, and to allow the complex amplitude of the interfering wave to vary as $F(u,v)$. Under these circumstances, the elementary fringe pattern, $I_f(x,y;u,v)$, has the form

$$I_f(x,y;u,v) = |R_o + F(u,v)e^{j2\pi(ux+vy)}|^2$$
$$= R_o^2 + |F(u\ v)|^2 + 2\mathrm{Re}\{R_o F(u,v)e^{j2\pi(ux+vy)}\} \qquad (1)$$

where Re{ } denotes the real part. As time progresses, u and v are scanned i.e., fringe patterns of different spatial frequencies (u,v) are produced. Assuming that u and v are scanned through the entire range for which F(u,v) is nonzero, the superposition of all such fringe patterns yields the integrated fringe pattern given below:

$$I(x,y) = \iint R_o^2 dudv + \iint |F(u,v)|^2 dudv$$
$$+ 2R_o\mathrm{Re}\{\iint F(u,v)e^{j2\pi(ux+vy)}dudv\}, \qquad (2)$$

The term in curly brackets is recognized to be the inverse Fourier transform of F(u,v), or f(x,y). Assuming this latter function is real - the case of interest here - the integrated fringe pattern is given by

$$I(x,y) = \mathrm{BIAS} + 2R_o f(x,y). \qquad (3)$$

Each fringe pattern entering into the synthesis of Fq. (2) has a contrast or visibility given by

$$V(u,v;R_o) = R_o|F(u\ v)|/(R_o^2+|F(u,v)|^2). \qquad (4)$$

In order to maximize the contrast of the integrated fringe pattern, we choose the reference wave amplitude R_o so as to maximize the average fringe visibility:

$$R_o = E\{|F(u,v)|\}. \qquad (5)$$

where E{ } denotes an average over all components actually entering into the synthesis. (because of the excessive bias, zero spatial frequency is omitted in the synthesis.) In order to gain some feel for the signal-to-bias ratio resulting from such a synthesis, we simulated the operation on a computer. The 256x256-pixel images shown in Fig. 3 served as input. In all three cases the input image intensity range was adjusted to have a minimum value of 0.0 and a maximum value of 1.0. Application of the constant reference synthesis algorithm to image (a) resulted in an output image with bias level equaling 147.0 and image signal fluctuations in the range 147.0 to 148.0. The visual contrast of such an image is so low that no image structure could be perceived. However, detectors of sufficient dynamic range are capable of measuring

A B C

Fig. 3. Test images used as inputs to numerical simulations.

extremely low contrast imagery. For example, charge coupled photo-diode arrays with dynamic ranges of approximately 12 bits, corresponding to a peak intensity of 4095 relative to unity rms noise fluctuations, are available. If such a detector were used to detect the low contrast, constant-reference synthesis corresponding to image (a), a post-detection bias subtraction would yield an image with 27 to 28 meaningful (in a signal-to-noise ratio sense) levels of display intensity. Stated differently, if the peak intensity of the low-contrast image is set equal to the maximum detectable relative intensity value, 4095, all image fluctuations occur in the top 28 levels of the detector range. The final output image thus has a dynamic range (peak intensity variation to rms noise fluctuation) of 28:1, or about 4.8 bits. Results for image (a), along with those for images (b) and (c), are summarized in Table 1.

TABLE 1

RESULTS - CONSTANT REFERENCE SYNTHESIS:

12 BITS OF DETECTOR DYNAMIC RANGE

IMAGE A:	27 to 28 levels of display - 4.8 bits
IMAGE B:	48 to 49 levels of display - 5.6 bits
IMAGE C:	49 levels of display 5.6 bits

Unity Contrast Fringe Synthesis

If a synthesized image of contrast higher than that achievable with the optimum constant reference synthesis is to be obtained it is necessary for both interfering waves to vary in amplitude. Highest possible image contrast (and, therefore, highest output signal-to-noise ratio) is achieved if each elemental fringe pattern has unity visibility or contrast. This condition is achieved if the interfering waves have the same magnitude, equal to the square root of $|F(u,v)|$. Such a synthesis is represented by Eq. (6), where the phase of the resultant fringe pattern is split between the interfering wave amplitudes:

$$I_f(x,y,u,v) = |F^{+\frac{1}{2}}(u,v) + F^{-\frac{1}{2}}(u,v)e^{j2\pi(ux+vy)}|^2$$

$$= |F(u,v)|\{1 + \cos[2\pi(ux+vy) + \arg\{F(u,v)\}]\}. \qquad (6)$$

Integrating over spatial frequency space, we obtain the integrated fringe pattern

$$I(x,y) = \iint|F(u,v)|dudv + \iint|F(u,v)|\cos\{2\pi(ux+vy) + \arg\{F(u,v)\}\}dudv, \qquad (7)$$

which again has the form $I(x,y) = BIAS + f(x,y)$ for real $f(x,y)$. When this kind of synthesis is simulated numerically (again excluding $u=v=0$ from the integration), images of considerably higher contrast result. In particular, such a synthesis applied to image (a) results in a biased image with minimum value 11.2 and peak value 12.2. If we assume a 4095:1 detector intensity dynamic range, 3760/4095 of the dynamic range is used up by bias, the remaining 335 detectible levels being available for image display. The dynamic range of the

final displayed image intensity distribution would thus be 335:1. Table 2 summarizes the results of such a synthesis for all three test images.

TABLE 2

RESULTS - UNITY CONTRAST FRINGE SYNTHESIS

12 BITS OF DETECTOR DYNAMIC RANGE

IMAGE A:	335 levels of display	8.4 bits
IMAGE B:	582 levels of display	9.2 bits
IMAGE C:	666 levels of display	9.4 bits

Effect of Increasing Image Spacebandwidth Product

It is well known from the study of incoherent holography that the signal-to-bias ratio of syntheses of this type decreases with an increase in the spacebandwidth product of the synthesis. It can be shown that, for fixed signal level, the bias for the unity fringe contrast synthesis increases in proportion to $SB \times E\{|F(u,v)|\}$, where SB denotes the spacebandwidth product of the synthesized image. For the constant reference case, bias increases in proportion to $SB \times (E\{|F|\} + E\{|F|^2\})/E\{|F|\}$. Recalling that our test images consisted of 256x256 pixels, we would expect roughly a 4:1 reduction in the dynamic range of more detailed 512x512-pixel images. Since such images have roughly the spacebandwidth product of TV images (actually, the spacebandwidth product of typical television images is perhaps only 75% of that of a 512x512 test image), these numbers are particularly significant. Dividing the dynamic ranges shown in Table 2 by a factor of four, we obtain the numbers presented in Table 3.

TABLE 3

512x512 IMAGERY WITH 12-BIT DETECTOR

TYPE A IMAGE:	89 levels or 6.5 bits
TYPE B IMAGE:	146 levels or 7.2 bits
TYPE C IMAGE:	167 levels or 7.4 bits

Conclusions

The numbers in Table 3, representing unity contrast fringe syntheses of 512x512 spacebandwidth-product imagery (assuming a detector with 12 bits of dynamic range for measuring image intensity values), can only be taken as rough indicators of what might be achieved with a given image. Nevertheless, these results are quite encouraging. Six to eight bits of gray level is generally considered adequate for high-quality image display, and our test results fall within that range for imagery of spacebandwidth product exceeding that of conventional television imagery. These results thus clearly indicate the acceptability of time-integration techniques for many image processing applications, so long as unity contrast fringe syntheses are employed. Note that (from Table 2) a constant reference synthesis would result in a 512x512 spacebandwidth product image display with dynamic range between three and four bits of gray level. Such displays would typically appear noisy to the observer.

It should be noted that imagery that has undergone significant processing, for example highpass or bandpass filtering, may exhibit significantly different statistics and result in imagery of display dynamic range that is substantially higher or lower than was the case for the three test images. We also point out that the bias reduction philosophy described in this paper is applicable not only to time-integration image processing, but also to time-integration spectral analysis and to time-integration holography [17,18].

The assistance of J. M. Florence in the numerical simulations is gratefully acknowledged. This work was supported by the U. S. Air Force Office of Scientific Research.

References

1. R. A. Sprague, C. L. Koliopoulos, "Time integration acousto-optic correlator," Appl. Opt. 15 (1976) 89-92.
2. R. Sprague, "A review of acoustooptic signal correlators," Opt. Engrng. 16 (1977) 467-474.
3. R. M. Montgomery, "Acousto-optic signal processing system," U. S. Patent 3 634 749, 1972.
4. T. Turpin, "Time integrating optical processors," in Real-Time Signal Processing, F. Tao, ed. (Proc. SPIE Vol. 154, 1978), pp. 196-203.
5. P. Kellman, "Detector integration acousto-optic signal processing," in Proceedings of the 1978 International Optical Computing Conference (Digest of Papers) (IEEE, 1978, No. 78CH1305-2C), pp. 91-95.
6. T. R. Bader, "Acousto-optic spectrum analysis: A high performance hybrid technique," Appl. Opt. 18 (1979) 1668-1672.
7. J. Cohen, "Ambiguity processor architecture using one-dimensional acousto-optic transducers," in Real-Time Signal Processing, F. Tao, ed. (Proc. SPIE, Vol. 180, 1979), pp.
8. P. Kellman, "Time integrating optical processors " in Optical Processing Systems, W. Rhodes, ed. (Proc. SPIE, Vol. 185, 1979), pp. 130-139.
9. T. R. Bader, "Coherent optical hybrid techniques for spectrum analysis," in Optical Processing Systems, W. Rhodes, ed. (Proc. SPIE, Vol. 185, 1979), pp. 140-146.
10. D. Psaltis, D. Casasent, "Time- and space-integrating spectrum analyzer," Appl. Opt. 18 (1979) 3203-3204.
11. P. Kellman, "Time-integration optical signal processing," Opt. Engrng. 19 (May-June 1980).
12. P. S. Guilfoyle, D. L. Hecht, D. L. Steinmetz, "Joint-transform time-integration acousto-optic correlator for chirp spectrum analysis," in Bulk Acoustic Wave Devices (Proc. SPIE, Vol. 214, 1980).
13. W. T. Rhodes, "Space-frequency conversions for image transmission and processing," Optics Lett. 3 (1978) 24-26.
14. W. T. Rhodes, "Image processing using space-to-temporal frequency conversion," in Proceedings of the 1978 Conference of the International Commission on Optics (Madrid, 1978), pp. 261-264.
15. W. T. Rhodes, "Acousto-optic devices applied to image processing," in Real-Time Signal Processing II, F. Tao, ed. (Proc. SPIE, Vol. 180, 1979), pp. 143-149.
16. W. T. Rhodes, "Fourier transform scanning hybrid image processor," in preparation.
17. M. O. Hagler, E. L. Kral, J. F. Walkup, "Linear coherent processing using an input scanning technique," in Proceedings of the 1978 International Optical Computing Conference (Digest of Papers) (IEEE, 1978, No. 78CH1305-2C), pp. 148-152.
18. R. J. Marks II, "Two-dimensional coherent space-variant processing using temporal holography: Processor theory," Appl. Opt. 18 (1979) 3670-3674.

Acousto-Optic Signal Processing: Convolution and Correlation

WILLIAM T. RHODES, MEMBER, IEEE

Invited Paper

Abstract—**The use of acousto-optic devices in real-time signal convolution and correlation has increased dramatically during the past decade because of improvements in device characteristics and implementation techniques. Depending on the application, processing can be implemented via spatial or temporal integration. Two-dimensional signal processing (including image processing) is possible, in spite of the inherent one-dimensional nature of the acousto-optic device as a spatial light modulator.**

I. Introduction

THE ACOUSTO-OPTIC cell has a long history of application to optical processing and display, dating back at least to the late 1930's when Okolicsanyi proposed its use in projection television systems [1]. References to its use in converting electrical signals into spatial light distributions appear in a number of early papers on optical signal processing [2]-[4], and in the 1960's extended research programs were conducted on its application to the processing of radar and telecommunications signals [5]-[16]. Various techniques developed during this period have been described by Maloney in a highly readable paper in *IEEE Spectrum* magazine [17]. Developments of new techniques since 1970 have significantly enhanced the capabilities of acousto-optic cells in specific signal processing tasks. For example, through the application of time-integration acousto-optic processing methods, processing time-bandwidth products greatly exceeding the time-bandwidth product of the acousto-optic device itself can be achieved, and spatial filtering of two-dimensional (2-D) distributions—e.g., image deblurring—is possible.

This paper presents a tutorial review of acousto-optic signal processing methods, particularly those developed during the 1970's, as they relate to the linear shift-invariant filtering operations of convolution and correlation, both 1-D and 2-D. (See [18] for a complementary discussion of acousto-optic methods in signal spectral analysis.) We place major emphasis on systems aspects, choosing examples to illustrate key points. A Fourier optics point of view is stressed throughout [19]-[21].

II. Use of Acousto-Optic Cells as Spatial Light Modulators

A. General Background

If the operation of different acousto-optic correlators and convolvers is to be understood, it is important that the basic relationship between the driving electrical signal and the resultant modulation of light waves, both spatially and temporally, be clear. In order to facilitate a better understanding of the systems described in later sections, we therefore first review the basic characteristics of acousto-optic cells as spatial light modulators. We begin by considering briefly certain physical constraints that bear on the types of signal waveforms that can serve as input and the ways in which acousto-optic cells can be used.

To begin with, acoustic waves launched by the transducer into the cell frequently cannot be viewed, or otherwise detected optically, if they are imaged in conventional fashion. Like an unstained amoeba under a microscope, the acoustic wave structure remains unseen unless some special technique, such as phase contrast imaging or dark central field imaging, is used to render it visible [19, ch. 7].

As another point of great operational importance, we note that the electrical signals that drive acousto-optic cells must generally be bandpass in nature, with frequency content typically in the range of 1 MHz to 1 GHz. Reasonably large fractional bandwidths are acceptable, depending on the nature of the acousto-optic material and the transducer [22]. This restriction on the input signal waveform means that signals to be processed, if not originally bandpass in nature, must be placed on carriers in order to be suitable for input. The carrier can be modulated in both magnitude and phase, allowing complex signal processing. In many cases, an acousto-optic cell can be used directly in processing of radar and RF communication signals without the need for additional modulation.

Finally, it should be recalled that physical size of the cell and attenuation of sound waves in the cell material limit the practical duration of the signal contained in the cell at one instant in time to, typically, a few tens of microseconds. This prevents the use of acousto-optic devices in many speech and other voiceband signal processing operations, where the minimum useful time window is typically tens of milliseconds. (An exception occurs in spectrum analysis, where time-integration acousto-optic processing methods can yield useful short-time spectra with time windows in the tens-of-milliseconds range.)

B. Analytical Modeling

When used as a spatial light modulator, an acousto-optic cell is illuminated by a beam of light, usually collimated, and the wave field of that beam is modified by the sound waves in the cell via diffraction processes. The nature of the acousto-optic interaction is influenced by the thickness, in the direction of

Manuscript received June 18, 1980; revised September 4, 1980. This work was supported by the U.S. Air Force Office of Scientific Research.
The author is with the School of Electrical Engineering, Georgia Institute of Technology, Atlanta, GA 30332.

0018-9219/81/0100-0065$00.75

light wave propagation, of the interaction region. Specifically, if this thickness is large compared to the distance between neighboring acoustic wavefronts in the cell, Bragg or volume effects are significant and conditions for diffraction of the incident light are modified. We begin by modeling "thin" interaction or Raman–Nath regime operation, then consider modifications necessary for Bragg regime modeling. Our analysis is 1-D in nature except where extension to two dimensions is necessary. In modeling the cell we assume that sound wave reflection at the end of the cell opposite the input transducer is suppressed, i.e., acoustic wave propagation is unidirectional.

With reference to Fig. 1, the signal-driven acousto-optic cell is characterized by a complex wave amplitude transmittance function $t(x,t)$, where x is the spatial coordinate along the axis of acoustic wave propagation and t denotes time. (We consistently use boldface notation to denote complex-valued quantities.) If we let $s(x)$ represent, to within a proportionality constant, the transducer-induced elastic strain field in the acousto-optic medium at time $t = 0$, $t(x,t)$ is given by [17]

$$t(x,t) = \exp\,[js(x - Vt)]\ \text{rect}\ (x/W) \tag{1}$$

where V is the velocity of the strain field in the medium (the acoustic velocity), W is the width of the cell, and rect$(\cdot)$ denotes the unit rectangle function. The origin of the x-axis is placed at the middle of the cell. The strain field at the transducer end of the cell, $s[-(W/2) - Vt]$, is proportional to the input signal voltage $v(t)$; i.e.,

$$s[-(W/2) - Vt] = mv(t) \tag{2}$$

where m is a proportionality constant. If (1) is rewritten in terms of $v(t)$, the resulting representation for $t(x,t)$ has the advantage of linking the acousto-optic cell transmittance and, thereby, any processor outputs directly to the input signal waveform. However, the form of (1) lends itself to a more compact analysis of the operation of processing systems considered initially and will, therefore, be used for the time being; i.e., $s(x - Vt)$ will itself in general be treated as the system input, with (2) providing the link to the driving electrical signal waveform. Pictorial reasoning is generally adequate in linking $s(x - Vt)$ and $v(t)$: if $s(\cdot)$ and $mv(\cdot)$ are plotted as functions of the same variable, they vary only by a horizontal scale factor (the sound velocity) and a delay (corresponding to the time required for the strain wave to propagate from the transducer to the optical axis at $x = 0$).

As suggested earlier, the driving signal waveform is normally an RF carrier that is modulated in magnitude and phase. We write the corresponding strain wave, for $t = 0$, as

$$s(x) = a(x)\cos\,[2\pi f_0 x + \alpha(x)]. \tag{3}$$

Substituting for $s(x - Vt)$ in (1) and expanding the exponential in a power series, we obtain (with H.O. denoting higher order in s)

$$\begin{aligned} t(x,t) &= \{1 + js(x - Vt) + \text{H.O.}\}\ \text{rect}\ (x/W) \\ &= \{1 + ja(x - Vt)\cos\,[2\pi f_0(x - Vt) \\ &\quad + \alpha(x - Vt)] + \text{H.O.}\}\ \text{rect}\ (x/W). \end{aligned} \tag{4}$$

If the modulation amplitude $a(x)$ can be assumed small, the higher order terms can be neglected,[1] and, on expanding the cosine into exponentials, we obtain

$$\begin{aligned} t(x,t) = \{&1 + ja(x - Vt)\exp\,[j\alpha(x - Vt)]\exp\,[j2\pi f_0(x - Vt)] \\ &+ ja(x - Vt)\exp\,[-j\alpha(x - Vt)] \\ &\cdot \exp\,[-j2\pi f_0(x - Vt)]\}\ \text{rect}\ (x/W), \end{aligned} \tag{5}$$

or, equivalently,

$$\begin{aligned} t(x,t) = \{&1 + ja(x - Vt)\exp\,[j2\pi f_0 x]\exp\,[-j2\pi\nu_0 t] \\ &+ ja^*(x - Vt)\exp\,[-j2\pi f_0 x]\exp\,[j2\pi\nu_0 t]\}\ \text{rect}\ (x/W) \end{aligned} \tag{6}$$

where ν_0 is the temporal frequency of the driving RF carrier, related to spatial frequency f_0 by $\nu_0 = f_0 V$, and where $a(x) = |a(x)|$, $\alpha(x) = \arg\{a(x)\}$.

It is of considerable use to us in later analyses to express the transmittance function $t(x,y)$ in terms of the analytic signal $\tilde{s}(x)$ associated with $s(x)$, defined by[2]

$$\tilde{s}(x) = a(x)\exp\,[j2\pi f_0 x]. \tag{7}$$

Then $s(x) = \text{Re}\{\tilde{s}(x)\}$, and

$$t(x,t) = \{1 + j(\tfrac{1}{2})\tilde{s}(x - Vt) + j(\tfrac{1}{2})\tilde{s}^*(x - Vt)\}\ \text{rect}\ (x/W). \tag{8}$$

Equations (6)–(8) serve as the principal basis for our subsequent analyses.

If the acousto-optic cell is illuminated by a monochromatic, normally incident, unit-amplitude plane wave, the complex wave amplitude of the transmitted wave $u(x,t)$ equals $t(x,t)$. It is instructive to consider the special case where $a(x - Vt) = 1$; *i.e., the driving waveform is an unmodulated carrier.* Under these circumstances, $u(x,t)$ is given by (from (6))

$$\begin{aligned} u(x,t) = \{&1 + j\exp\,[j2\pi f_0 x]\exp\,[-j2\pi\nu_0 t] \\ &+ j\exp\,[-j2\pi f_0 x]\exp\,[j2\pi\nu_0 t]\}\ \text{rect}\ (x/W). \end{aligned} \tag{9}$$

Let ν denote the optical frequency of the incident wave ($\sim 5 \times 10^{14}$ Hz): $\nu = c/\lambda$, c = speed of light, λ = wavelength. If we ignore the effects of the window function, the three terms of (9) represent, respectively, an undiffracted component at optical frequency ν traveling in the $+z$ direction (the zeroth order); a diffracted plane wave component at optical frequency $(\nu - \nu_0)$ with propagation direction inclined through angle $\sin^{-1}(\lambda f_0)$ toward the $+x$-axis (the -1 order, taking the sign in accord with the frequency shift) and a diffracted plane wave component at optical frequency $(\nu + \nu_0)$ with propagation direction inclined through angle $\sin^{-1}(\lambda f_0)$ away from the $+x$-axis (the $+1$ order). The directions of propagation and respective optical frequencies are noted in Fig. 1. The shift in frequency of the diffracted waves can be viewed in terms of conservation of photon and phonon momentum, Doppler shift, or as a natural consequence of the diffraction process. All points of view lead to the same result. The Doppler shift point of view is attractive in that it gives us on inspection the sign of the frequency shift.

The trio of diffraction orders in (9) (and the neglected higher order components as well) is characteristic of Raman–Nath regime operation of an acousto-optic cell. As Bragg regime operation is approached, either through an increase in acoustic frequency ν_0 or through a broadening of the acoustic beam,

[1] To the extent that $a(x)$ is not small, intermodulation products become significant and can, in some cases, adversely affect device performance. For an analysis see [23].

[2] Strictly speaking, $s(x)$ is not an analytic signal as defined, but rather the exponential representation signal associated with $s(x)$. However, the difference between the two is ignorable for the narrow-band case of concern. See [24].

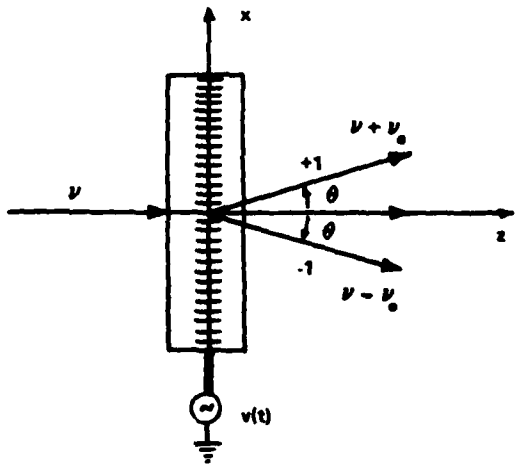

Fig. 1. Acousto-optic cell showing directions and center frequencies of diffracted waves.

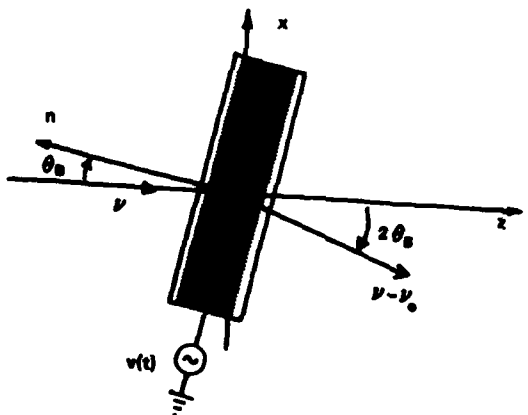

Fig. 2. Geometry for diffraction in Bragg regime.

the diffraction efficiency for normally incident illumination diminishes, ultimately to an insignificant level. To observe diffraction again, it is necessary to rotate the cell slightly in its plane, as shown in Fig. 2, until the angle the incident beam makes with the cell satisfies the Bragg condition:

$$\theta_B = \sin^{-1}(\lambda/2\Lambda) \tag{10}$$

where Λ is the acoustic wavelength. In this regime, only one of the first order diffraction components is produced with significant magnitude. For the case illustrated in Fig. 2, this is the downshifted or -1 component at frequency $(\nu - \nu_0)$, and the effective transmittance of the cell can be represented by[3]

$$\begin{aligned} t(x,t) &= \{1 + ja(x - Vt)\exp[j2\pi f_0 x] \\ &\quad \cdot \exp[-j2\pi\nu_0 t]\}\ \text{rect}\,(x/W) \\ &= \{1 + j(\tfrac{1}{2})\tilde{s}(x - Vt)\}\ \text{rect}\,(x/W). \end{aligned} \tag{11}$$

If the cell is rotated through θ_B in the opposite direction, it is the upshifted or +1 diffraction component that is produced, and $t(x,t)$ can be represented by

$$\begin{aligned} t(x,t) &= \{1 + ja^*(x - Vt)\exp[-j2\pi f_0 x] \\ &\quad \cdot \exp[j2\pi\nu_0 t]\}\ \text{rect}\,(x/W) \\ &= \{1 + j(\tfrac{1}{2})\tilde{s}^*(x - Vt)\}\ \text{rect}\,(x/W). \end{aligned} \tag{12}$$

As noted by Korpel [25], relatively large fractional bandwidths for the complex modulation $a(x - Vt)$ can be accommodated while good Bragg discrimination against other orders is retained if phased array transducers are used. Bragg regime operation is common in acousto-optic processing, particularly since the 1960's, because of the greater diffraction efficiency that is generally possible. In particular, the modulation level $a(x - Vt)$ can be increased significantly without the production of complicating higher order diffraction components.

C. Phase to Amplitude Conversion

Essential for the operation of most acousto-optic processing systems is the conversion at one stage or another in the system of the temporal and spatial *phase* modulation of light, represented by (1), into some form of temporal and spatial modulation of light wave *intensity*. This can be accomplished in several ways using the spatial filtering system of Fig. 3. The cell is illuminated by a collimated beam of light; in the back focal plane of lens L_1 appears the spatial Fourier transform of $t(x,t)$. Successful operation of the spatial filtering system depends on the physical separation in the spatial filter plane of the Fourier transforms of the three terms of (7). This separation is assured by the bandpass nature of $s(x - Vt)$, and requires only that the spatial bandwidth of the modulation $a(x - Vt)$ be smaller than f_0 (equivalently, that the cutoff temporal frequency of $a(x - Vt)$ be smaller than ν_0), a condition virtually always satisfied in acousto-optic cell operation.

Two principal methods of conversion are described. Additional methods are described in [26]. *In the Zernike phase contrast method*, the optical phase of the undiffracted wave from the cell is shifted by 90° by a quarter-wave plate on the optical axis in the spatial filter plane. The result is an output plane wave amplitude given by (from (4))

$$u(x,t) = \{j + js(x - Vt)\}\ \text{rect}\,(x/W),$$

with corresponding intensity, given by $|u(x,t)|^2$, equal to

$$I(x,t) = \{1 + 2s(x - Vt) + s^2(x - Vt)\}\ \text{rect}\,(x/W). \tag{13}$$

As desired, this intensity distribution contains the signal term $s(x - Vt)$. The output of a small photodetector at point x in the image plane will be proportional to $I(x,t)$. Only $s(x - Vt)$ itself contains temporal frequency content about the carrier frequency ν_0; thus, if the detector output is bandpass filtered, an output electrical waveform proportional to a delayed version of $v(t)$ can be obtained.

In the *half-plane stop method*, either the +1 or the -1 diffraction order is blocked in the spatial filter plane, with the resultant output intensity (with a +1 order stop)

$$\begin{aligned} I(x,t) &= |1 + j(\tfrac{1}{2})\tilde{s}(x - Vt)|^2\ \text{rect}\,(x/W) \\ &= \{1 + (\tfrac{1}{4})a^2(x - Vt) + 2s(t)\}\ \text{rect}\,(x/W). \end{aligned} \tag{14}$$

Again, a bandpass filter following the output of a small image plane detector yields the modulation waveform, since the second term is low-pass in nature. If the acousto-optic cell is operating in the Bragg regime, no such filtering is required, the second diffraction component being naturally suppressed.

[3] A more accurate model would include a complex constant of proportionality with the second term.

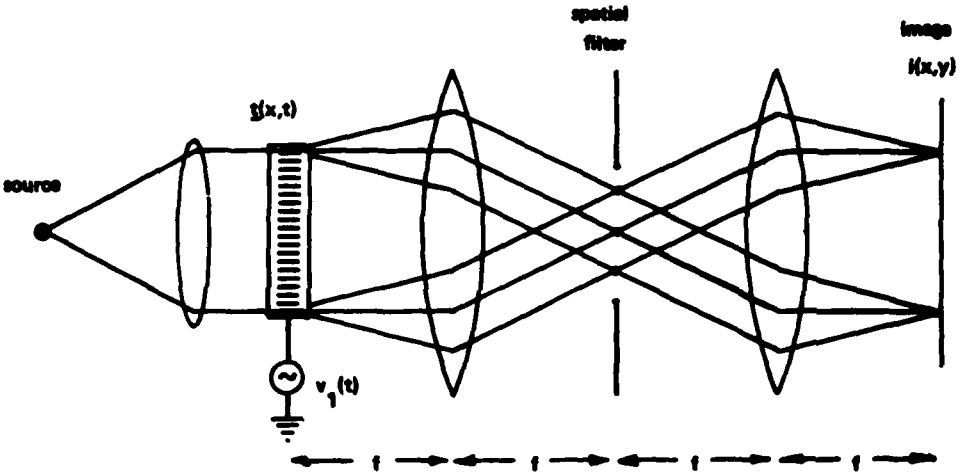

Fig. 3. Use of spatial filtering system to convert phase modulation to amplitude modulation.

It is important to note that neither complete temporal nor complete spatial coherence is required of the wave illuminating the acousto-optic cell in order for these conversion processes to operate, and indeed this is true of most of the correlators and convolvers to be discussed. This is evident if we consider the effects on the spatial filter plane distributions in Fig. 3 of enlarging the source of broadening its spectral bandwidth. In either case, the result is a smearing out of the three diffraction components in the Fourier plane. However, so long as these distributions *do not overlap spatially, the desired filtering* operation can still be performed. (For broad-band sources, it is necessary to use achromatic wave plates in the phase shifting methods.)

There are alternative methods for modulation conversion that do not require spatial filtering. For example, Meltz and Maloney note that simple propagation of the transmitted optical wave distribution through a distance $Z_\cdot = \lambda^2/2\Lambda$ leads to the same result as the Zernike phase contrast method discussed above, assuming satisfactorily small modulation bandwidth [14]. In addition, if shear-wave acousto-optic cells are employed (for example, TeO_2), lensless conversion methods using birefringent waveplates and polarizers can be employed [16].

III. 1-D Space Integrating Convolvers and Correlators

A. Notation and Basic Relationships

Given two real-valued distributions $s_1(x)$ and $s_2(x)$, we desire to evaluate either their convolution or their cross correlation. Since the two operations are related through simple coordinate reversals, we concentrate on the cross correlation, this being the operation of greatest interest in radar and RF communications signal processing. In acousto-optic processing, $s_1(x)$, $s_2(x)$, and, therefore, their cross correlation are narrow-band signals—carriers modulated, in general, both in magnitude and in phase. As we shall see, acousto-optic correlators can be constructed to yield as output either the envelope of the correlation function or the entire complex modulated carrier.

Before considering specific examples of systems, we establish some basic notation and relationships for the correlation integral. The cross correlation of real s_1 and s_2 is given by (infinite limits are assumed unless otherwise noted)

$$R_{12}(\tau) = \int s_1(x)\, s_2(x+\tau)\, dx \tag{15a}$$

$$= \int s_1(x-\tau)\, s_2(x)\, dx. \tag{15b}$$

Following the notation established in Section II, we write

$$s_1(x) = a_1(x)\cos\left[2\pi f_0 x + \alpha_1(x)\right] \tag{16a}$$

$$= \mathrm{Re}\left\{\tilde{s}_1(x)\right\} \tag{16b}$$

$$s_2(x) = a_2(x)\cos\left[2\pi f_0 x + \alpha_2(x)\right] \tag{17a}$$

$$= \mathrm{Re}\left\{\tilde{s}_2(x)\right\} \tag{17b}$$

where $\tilde{s}_1$ and $\tilde{s}_2$ are the analytic signals associated with s_1 and s_2, respectively. Exploiting the properties of the analytic signal representation, one can write the correlation of real waveforms $s_1(t)$ and $s_2(t)$ in terms of a complex correlation of $\tilde{s}_1(t)$ and $\tilde{s}_2(t)$:[4]

$$R_{12}(\tau) = (\tfrac{1}{2})\,\mathrm{Re}\left\{\int \tilde{s}_1^*(x-\tau)\tilde{s}_2(x)\,dx\right\} \tag{18a}$$

$$= (\tfrac{1}{2})\,\mathrm{Re}\left\{\exp\left[j2\pi f_0\tau\right]\int a_1^*(x-\tau)a_2(x)\,dx\right\} \tag{18b}$$

$$= (\tfrac{1}{2})\,\mathrm{Re}\left\{\exp\left[j2\pi f_0\tau\right] r_{12}(\tau)\right\} \tag{18c}$$

$$= (\tfrac{1}{2})\, r_{12}(\tau)\cos\left[2\pi f_0\tau + \theta_{12}(\tau)\right] \tag{18d}$$

where

$$r_{12}(\ ) = \int a_1^*(x-\tau)a_2(x)\,dx \tag{18e}$$

$$r_{12}(\tau) = |r_{12}(\tau)| \tag{18f}$$

$$\theta_{12}(\tau) = \arg\left\{r_{12}(\tau)\right\}. \tag{18g}$$

[4] The proof is relatively easy if it is remembered that the analytic signal contains only positive frequency components.

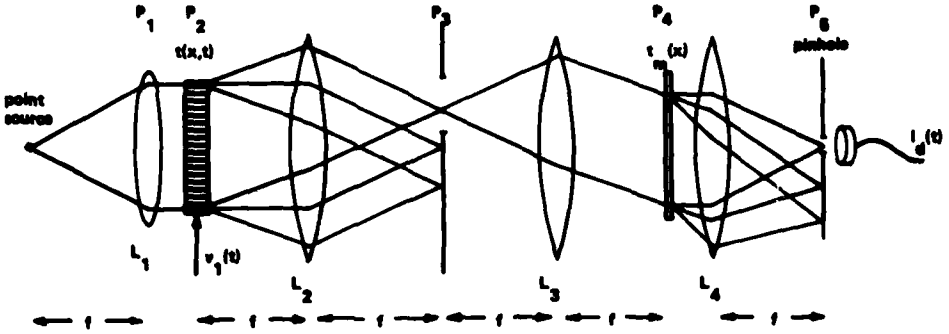

Fig. 4. Nonheterodyning correlator/convolver with single doubly diffracted component incident on pinhole detector.

It should be noted that a_1 and a_2 can represent real baseband signals (which are placed on a carrier for acousto-optic modulation) if α_1 and α_2 equal zero or pi. In that case, $R_{12}(\tau)$ is a pure amplitude-modulated carrier with the amplitude conveying the correlation of $a_1(x)$ and $a_2(x)$.

B. Nonheterodyning Space-Integrating Correlator

In the traditional form of acousto-optic correlator, the integral of (15) is an integration over a spatial coordinate. As a first example of a space-integrating correlator, consider the system of Fig. 4, which evaluates the square of the correlation envelope $r_{12}(\tau)$. The acousto-optic cell can be operated in the Bragg regime, though we assume Raman–Nath operation in our analysis. The complex wave amplitude of the cell is assumed to be given by (1) with $s(x - Vt) = s_1(x - Vt)$. The spatial filter mask in plane P_3 is constructed to pass only the frequency-upshifted +1 diffraction component, and the wave amplitude incident on the mask in plane P_4 therefore has the form (note that the sense of the x-axis has been reversed in this plane, consistent with the inversion undergone in imaging plane P_2 to plane P_4):

$$u_{\text{inc}}(x, t) = (\tfrac{1}{2})\tilde{s}_1^*(x - Vt)\ \text{rect}\ (x/W). \tag{19}$$

The mask itself, which may be a phototransparency, is represented by amplitude transmittance

$$t_m(x) = [1 + s_2(x)]$$
$$= [1 + (\tfrac{1}{2})\tilde{s}_2(x) + (\tfrac{1}{2})\tilde{s}_2^*(x)]. \tag{20}$$

The absence of a factor j in the second and third terms is consistent with the amplitude modulation characteristics of photomasks.

The wave transmitted by the mask has complex amplitude

$$u_{\text{trans}}(x, t) = u_{\text{inc}}(x, t)\, t_m(x)$$
$$= \{(\tfrac{1}{2})\tilde{s}_1^*(x - Vt) + (\tfrac{1}{4})\tilde{s}_1^*(x - Vt)\tilde{s}_2(x)$$
$$+ (\tfrac{1}{4})\tilde{s}_1^*(x - Vt)\tilde{s}_2^*(x)\}\ \text{rect}\ (x/W). \tag{21}$$

To within a quadratic phase factor, the final lens Fourier transforms this distribution and the pinhole samples the resultant transform distribution at the origin, i.e., at zero spatial frequency. Of the three terms of (21), the first contains spatial carrier term exp $[-j2\pi f_0 x]$ and the third contains exp $[-j2\pi 2f_0 x]$. Only the second term, corresponding to a doubly diffracted wave component, has spatial frequency content about zero spatial frequency, and the wave amplitude

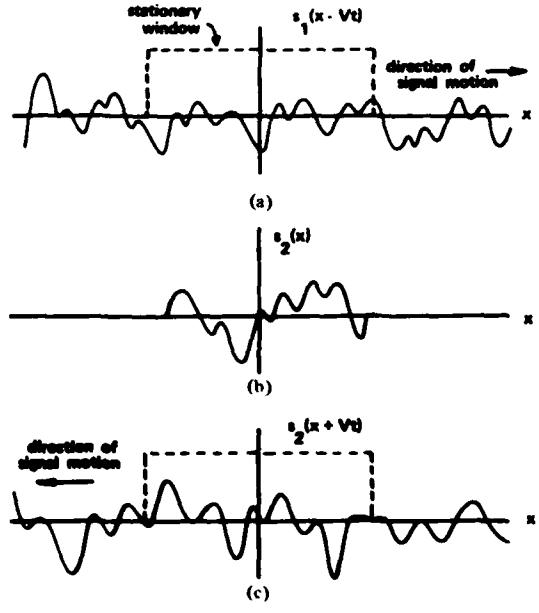

Fig. 5. Functions involved in correlation operation.

at the pinhole is thus given by

$$u_{\text{pinhole}}(t) = (\tfrac{1}{4})\int \tilde{s}_1^*(x - Vt)\tilde{s}_2(x)\ \text{rect}\ (x/W)\, dx. \tag{22}$$

Except for the window function, this function is proportional to $r_{12}(Vt)\exp[j2\pi\nu_0 t]$. The detector output $i_d(t)$ is proportional to the wave intensity $|u_{\text{pinhole}}|^2$; thus to the extent that the windowing effect of the finite cell length can be ignored (and dropping a proportionality constant),

$$i_d(t) = r_{12}^2(Vt). \tag{23}$$

It should be noted that this system requires illumination from a point source because of the pinhole detection arrangement. The source may, however, have broad spectral bandwidth, subject to the spatial filtering requirements in plane P_3.

In a closely related system, the photomask is replaced with a second acousto-optic cell, driven from the bottom. Taking the axis inversion into account, the mask transmittance then becomes

$$t_m(x, t) = 1 + j\tilde{s}_2(x + Vt) + j\tilde{s}_2^*(x + Vt). \tag{24}$$

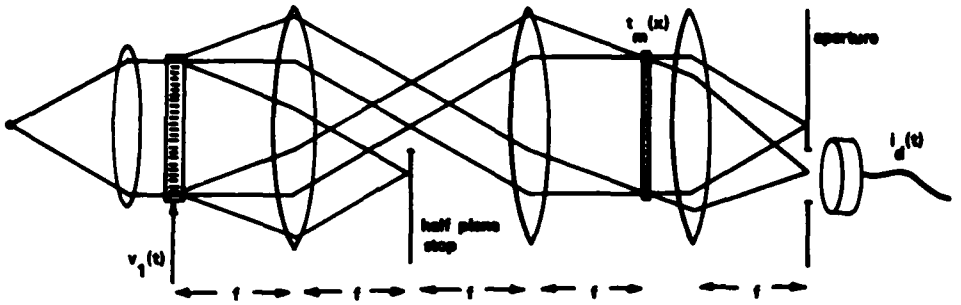

Fig. 6. Heterodyning correlator/convolver with zero and +1 diffraction component imaged on reference mask $t_m(x)$.

Proceeding as before, we find the detector output to be proportional to $r_{12}^2(2Vt)$, or, if the sound velocities are different, to $r_{12}^2[(V_1 + V_2)t]$, where the meaning of V_1, V_2 is obvious. Two-cell systems are convenient in that no photomask recording is required. It should be noted, however, that if such a system is to be used to correlate electrical signal waveforms $v_1(t)$ and $v_2(t)$, it is a *time-reversed* version of $v_2(t)$ that must drive the second acousto-optic cell. (This can be seen by considering the form of the spatial pattern induced in the cell that results, e.g., from a frequency-chirped input signal.) In certain cases a time-reversed version of $v_2(t)$ may be difficult to produce.

Window-imposed limitations on space-integration correlator (and convolver) operation are illustrated with the help of Fig. 5, which shows (a) the signal $s_1(x - Vt)$ moving past the window function, (b) the stationary phototransparency signal $s_2(x)$, and (c) acousto-optic signal $s_2(x + Vt)$ moving under a window. In order for the window to be ignorable, signal $s_1(x)$ must be no wider in extent than window width W. For matched filtering operations, this means that the duration T of the signal to be filtered should not exceed the acoustic transit time across the cell W/V. As noted earlier, this transit time rarely exceeds several tens of microseconds. For signals of greater duration, only partial correlation is possible with the space-integration method.

C. Heterodyning Correlators

With only minor modifications, the system of Fig. 4 can be made to yield the complete phase-bearing correlation function $R_{12}(\cdot)$ as output, not simply its envelope $r_{12}(\cdot)$. Processors that do this are generally referred to as heterodyne processors, since the information-bearing carrier is produced by the heterodyne mixing of two optical waves at the detector. For the example shown in Fig. 6, we allow the zeroth order to be passed by the spatial filter and replace the pinhole in front of the detector with an off-axis opening to pass one of the diffraction components. For analytical convenience we also introduce a 90° phase shift in the +1 diffraction component, although this is not essential. Proceeding as before but including the zeroth-order diffraction component, we have for the wave field transmitted by the mask

$$u_{\text{trans}}(x, t) = \{[1 + (\tfrac{1}{2})\tilde{s}_1^*(x - Vt)] \cdot [1 + (\tfrac{1}{2})\tilde{s}_2(x) + (\tfrac{1}{2})\tilde{s}_2^*(x)]\} \text{ rect } (x/W). \quad (25)$$

Of the various product terms, only the singly diffracted components $(\frac{1}{2})\tilde{s}_1^*(x - Vt)$ and $(\frac{1}{2})\tilde{s}_2^*(x)$, both of which contain spatial carrier terms $\exp[-j2\pi f_0 x]$, travel in the correct nominal direction to pass the detector plane mask. Thus so far as the detector is concerned, we need consider only the wave field

$$u_d(x, t) = \{(\tfrac{1}{2})\tilde{s}_1^*(x - Vt) + (\tfrac{1}{2})\tilde{s}_2^*(x)\} \text{ rect } (x/W). \quad (26)$$

Since the detector responds only to the time varying energy flow in this wave field, we can write for $i_d(t)$, the detector output,

$$\begin{aligned} i_d(t) &= \int |u_d(x, t)|^2 \, dx \\ &= (\tfrac{1}{4}) \int |\tilde{s}_1^*(x - Vt)|^2 \text{ rect } (x/W) \, dx \\ &\quad + (\tfrac{1}{4}) \int |\tilde{s}_2^*(x)|^2 \text{ rect } (x/W) \, dx \\ &\quad + (\tfrac{1}{2}) \text{ Re} \left\{ \int \tilde{s}_1^*(x - Vt)\tilde{s}_2(x) \text{ rect } (x/W) \, dx \right\}. \end{aligned} \quad (27)$$

The third term is, again to within limitations imposed by the window function rect (x/W), the desired cross correlation $R_{12}(Vt)$. Since $R_{12}(Vt)$ rides on a temporal frequency carrier $\nu_0 = Vf_0$, it can be separated by bandpass filtering from both the second term, which is at dc, and from the first term, which is a baseband term with twice the bandwidth of the modulation $a_1(t)$. As before, a second acousto-optic cell can be used for the signal s_2 as well.

A characteristic common to all heterodyning correlators and convolvers is the mixing at the detector of light waves with optical frequencies in two distinct bands (in the above case separated nominally by ν_0). In an alternate scheme described by Sprague in a review of acousto-optic correlators [27], the basic system of Fig. 4 is used, with the spatial filter passing the +1 and −1 diffraction components from the acousto-optic cell (shifted by $\pm\nu_0$, respectively) and blocking the zeroth order. The complex amplitude of the light wave transmitted by the mask is proportional to

$$u_{\text{trans}}(x, t) = \{[(\tfrac{1}{2})\tilde{s}_1(x - Vt) + (\tfrac{1}{2})\tilde{s}_1^*(x - Vt)] \cdot [1 + (\tfrac{1}{2})\tilde{s}_2(x) + (\tfrac{1}{2})\tilde{s}_2^*(x)]\} \text{ rect } (x/W). \quad (28)$$

In this case, only the product terms $(\frac{1}{4})\tilde{s}_1(x - Vt)\tilde{s}_2^*(x)$ and $(\frac{1}{4})\tilde{s}_1^*(x - Vt)\tilde{s}_2(x)$ have nominal propagation directions along the z-axis. Thus the complex wave amplitude at the on-axis

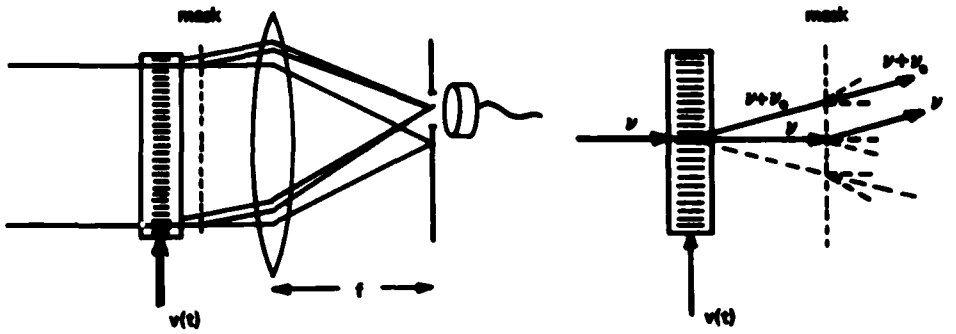

(a) (b)

Fig. 7. Proximity imaging, or compact correlator/convolver: (a) basic system; (b) diagram showing relative optical frequencies and origins of components that reach detector.

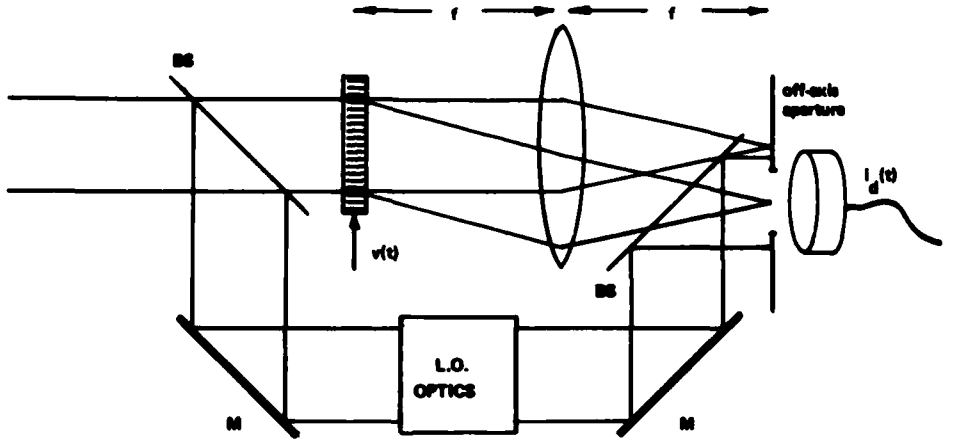

Fig. 8. Fourier plane heterodyne processor: M = mirror and BS = beamsplitter.

pinhole is given by

$$u_{\text{pinhole}}(t) = (\tfrac{1}{4}) \int [\tilde{s}_1^*(x - Vt)\tilde{s}_2(x) + \tilde{s}_1(x - Vt)\tilde{s}_2^*(x)] \operatorname{rect}(x/W)\, dx$$
$$= (\tfrac{1}{2}) \operatorname{Re}\left\{ \int \tilde{s}_1^*(x - Vt)\tilde{s}_2(x) \operatorname{rect}(x/W)\, dx \right\}. \quad (29)$$

Ignoring the window effect, this is the desired correlation. The detector, responding to the intensity of the light at the pinhole, has output

$$i_d(t) = |R_{12}(Vt)|^2 = r_{12}^2(Vt) \cos^2 [2\pi\nu_0 t + \theta_{12}(Vt)]$$
$$= (\tfrac{1}{2}) r_{12}^2(Vt) + (\tfrac{1}{2}) r_{12}^2(vT) \cos [2\pi 2\nu_0 t + 2\theta_{12}(Vt)]. \quad (30)$$

The second term, on a carrier, can be extracted by bandpass filtering. Some additional processing is required to obtain $r_{12}(Vt)$ and, if desired, $\theta_{12}(Vt)$ as final outputs.

A number of heterodyne correlators have been described that do not require the careful imaging of the acousto-optic cell onto the phototransparency that is characteristic of the systems of Figs. 4 and 6. An example is illustrated in Fig. 7. In this case the cell and mask are assumed to be sufficiently close together that they can be characterized by the product transmittance

$$t_{\text{prod}}(x, t) = t(x, t)\, t_m(x)$$
$$= \{[1 + (\tfrac{1}{2}) \exp [j\theta]\, \tilde{s}_1(x - Vt) + (\tfrac{1}{2}) \exp [j\theta]\, \tilde{s}_1^*(x - Vt)] \cdot [1 + (\tfrac{1}{2})\tilde{s}_2(x) + (\tfrac{1}{2})\tilde{s}_2^*(x)]\} \operatorname{rect}(x/W). \quad (31)$$

The phase factor $\exp [j\theta]$, which depends on the distance separating the mask and the acousto-optic cell, is chosen for convenience in analysis to equal $-j$. (For some other choice, the phase of the carrier of the cross correlation function changes.) With normally incident illumination of the acousto-optic cell, the light that passes the detector plane mask corresponds to the product terms containing spatial carriers of the form $\exp [j2\pi f_0 x]$, or the terms $(\tfrac{1}{2})\tilde{s}_1(x - Vt)$ and $(\tfrac{1}{2})\tilde{s}_2(x)$. The energy flux associated with these two waves, which governs the detector output, is given by

$$i_d(t) = \int |(\tfrac{1}{2})\tilde{s}_1(x - Vt) + (\tfrac{1}{2})\tilde{s}_2(x)|^2 \operatorname{rect}(x/W)\, dx \quad (32)$$

which evaluates to the same form as (27).

In order for this kind of correlator (sometimes referred to as a compact configuration correlator) to function correctly, it is necessary that the basic form of the wavefield transmitted by the acousto-optic cell not change significantly over the propagation distance separating cell and mask. This in turn imposes constraints on that distance and on the bandwidth of the complex modulation $a_1(\cdot)$ [14]. This kind of processor geometry has been exploited extensively by researchers at the Harry Diamond Laboratory with planar Bragg mode acousto-optic processors, typically with a second, reverse direction acousto-optic device replacing the phototransparency [28].

D. Fourier-Plane Heterodyne Processing

We close this section with a description of one additional type of space-integrating optical processor, investigated by Whitman *et al.* [15], that emphasizes the diversity of ways in which acousto-optic cells can be employed for signal filtering. Shown in Fig. 8, this system places the detector in the Fourier transform plane of the acousto-optic cell, behind a mask that passes only the −1 diffraction component. Incident on the detector are two wave distributions, one given by the spatial Fourier transform of the distribution $\tilde{s}_1(x - Vt)$, the other—referred to as the local oscillator (L.O.) wave—being determined by the nature of the optical system in the second arm of the optical system. Letting ξ denote the Fourier plane coordinate and denoting the L.O. wave (for reasons that will become clear) by $(\frac{1}{2})\tilde{S}_2^*(-\xi)$, we thus have for the wave amplitude at the detector

$$u_d(\xi, t) = (\tfrac{1}{2})\tilde{S}_1(\xi)\exp[-j2\pi\xi Vt] + (\tfrac{1}{2})\tilde{S}_2^*(-\xi) \quad (33)$$

where $\tilde{S}_1(\xi)\exp[-j2\pi\xi Vt]$ is the spatial transform of signal distribution $\tilde{s}_1(x - Vt)$. The detector output is given by

$$i_d(t) = \int |u_d(\xi, t)|^2\, d\xi \quad (34)$$

which, by Rayleigh's theorem, can be written as

$$i_d(t) = \int |(\tfrac{1}{2})\tilde{s}_1(x - Vt) + (\tfrac{1}{2})\tilde{s}_2^*(x)|^2\, dx$$

$$= (\tfrac{1}{4})\int |\tilde{s}_1(x - Vt)|^2\, dx + (\tfrac{1}{4})\int |\tilde{s}_2^*(x)|^2\, dx$$

$$+ (\tfrac{1}{2})\,\mathrm{Re}\left\{\int \tilde{s}_1(x - Vt)\tilde{s}_2(x)\, dx\right\} \quad (35)$$

where $\tilde{s}_2(x)$, the inverse spatial transform of $\tilde{S}_2(\xi)$, is the analytic signal associated with real signal $s_2(x)$. The first term of (35) is at baseband, the second at dc. The properties of analytic signals are such that the third, or ac term, denoted $i_{ac}(t)$, has the form of a convolution,

$$i_{ac}(t) = \int s_1(x - Vt)s_2(x)\, dx. \quad (36)$$

As a function of time, this term represents a filtered version of the input signal waveform $v_1(t)$, with the filter impulse response being governed by the function $s_2(x)$.

As noted in [15], a signal $v(t) = \cos 2\pi\nu_s t$ input to the acousto-optic cell produces a single spot of light, downshifted in frequency by ν_s, at point $\xi = \xi_s$ on the detector. This spot mixes with the wave $\tilde{S}_2^*(-\xi)$ at point $\xi = \xi_s$ to produce an output beat signal. This beat signal is itself sinusoidal at frequency ν_s; however, its magnitude and phase are governed by the magnitude and phase of the L.O. wave at point ξ_s. Thus, $\tilde{S}_2(\xi)$ plays the role of a transfer function, leading to an alternate point of view of the processor. In [29], Korpel establishes various basic relationships between this transfer function point of view and the convolution point of view. Recently Florence and Rhodes [30] have described a generalization of the Fourier plane heterodyne processor wherein the L.O. wave field varies in optical frequency as a function of Fourier plane coordinate ξ. The mixing processes that result lead to signal input–output relationships described loosely as a nonlinear mapping of signal frequency components. The method can be used for certain kinds of bandwidth compression and expansion.

IV. 1-D Time-Integrating Convolvers and Correlators

A. Introduction

Acousto-optic processors are well suited to wide-band signal processing, with acousto-optic correlators being particularly applicable to radar signal processing. Situations arise, however—for example, in direction finding of noise-like sources—where correlation times exceeding the transit time of the acousto-optic window are desirable or necessary. Extensions of the basic space-integrating methods discussed above have been investigated where correlation times are increased by the use of multiple cells with delay lines and by the use of folded-path acousto-optic devices [31]. Especially important in extending the capabilities of acousto-optic devices has been the development of an alternate class of acousto-optic processors, known collectively as time-integrating processors, that allow integration times of the order of tens of milliseconds and greater [32]–[41].

B. Two-Cell System

We begin with a description of the first processor of this class to be developed, reported by Montgomery in [32] and illustrated in Fig. 9. Because time-integration processing is characterized by integrations with respect to time rather than space, we modify our point of view from that taken in the previous section and emphasize t, the integration variable, by writing the acousto-optic cell transmittance directly in terms of the driving signal waveforms, $v_1(t)$ and $v_2(t)$. For convenience of notation we also move the x-axis origin from the optical axis to the bottom end of the cells. Under these circumstances, we can write (omitting a modulation proportionality constant and the window function)

$$t_1(x, t) = \exp[jv_1(t - x/V)] \quad (37a)$$

$$\doteq [1 + jv_1(t - x/V)] \quad (37b)$$

$$t_2(x, t) = \exp[jv_2(t + x/V - T)] \quad (38a)$$

$$\doteq [1 + jv_2(t + x/V - T)] \quad (38b)$$

where

$$v_1(t) = b_1(t)\cos[2\pi\nu_0 + \beta_1(t)] \quad (39)$$

$$v_2(t) = b_2(t)\cos[2\pi\nu_0 t + \beta_2(t)]. \quad (40)$$

In (38) the + sign denotes the reversed sound wave propagation direction, and T is the cell transit time W/V.

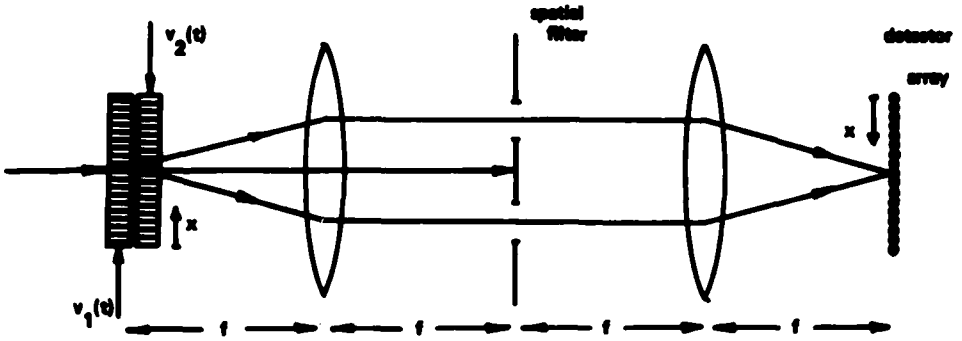

Fig. 9. Example of a two-cell time-integrating correlator/convolver. Rays show directions of principal diffraction components.

As before, we introduce the analytic signal representations for v_1, v_2, writing

$$v_1(t) = \text{Re}\,\{\tilde{v}_1(t)\} \tag{41}$$

$$v_2(t) = \text{Re}\,\{\tilde{v}_2(t)\} \tag{42}$$

where

$$\tilde{v}_1(t) = b_1(t)\exp[j\beta_1(t)]\exp[j2\pi\nu_0 t] \tag{43a}$$

$$= b_1(t)\exp[j2\pi\nu_0 t] \tag{43b}$$

$$\tilde{v}_2(t) = b_2(t)\exp[j\beta_2(t)]\exp[j2\pi\nu_0 t] \tag{44a}$$

$$= b_2(t)\exp[j2\pi\nu_0 t]. \tag{44b}$$

In terms of the analytic signals, the transmittance functions become

$$t_1(x,t) = \{1 + j(\tfrac{1}{2})\tilde{v}_1(t - x/V) + j(\tfrac{1}{2})\tilde{v}_1^*(t - x/V)\} \tag{45}$$

$$t_2(x,t) = \{1 + j(\tfrac{1}{2})\tilde{v}_2(t + x/V - T) + j(\tfrac{1}{2})\tilde{v}_2^*(t + x/V - T)\}. \tag{46}$$

Although the notation has been changed from that of Section III, it is important to note that the analytic signal terms $\tilde{v}_1$, $\tilde{v}_2$, $\tilde{v}_1^*$, and $\tilde{v}_2^*$ correspond directly to the acoustic wave terms $\tilde{s}_1$, $\tilde{s}_2$, $\tilde{s}_1^*$, and $\tilde{s}_2^*$ of earlier analyses. Specifically, as functions of x they lead to the same diffracted wave components as before and can be filtered out by appropriate spatial filter plane stops.

As a function of the real signals $v_1(t)$ and $v_2(t)$, the cross-correlation function $R_{12}(\tau)$ has the form

$$R_{12}(\tau) = \int v_1(t - \tau)\, v_2(t)\, dt \tag{47}$$

which in terms of the analytic signals can be written as

$$R_{12}(\tau) = (\tfrac{1}{2})\,\text{Re}\left\{\int \tilde{v}_1^*(t - \tau)\,\tilde{v}_2(t)\, dt\right\} \tag{48a}$$

$$= (\tfrac{1}{2})\,\text{Re}\,\{\exp[j2\pi\nu_0\tau]\, r_{12}(\tau)\} \tag{48b}$$

where

$$r_{12}(\tau) = \int b_1^*(t - \tau)\, b_2(t)\, dt. \tag{49}$$

In practice, the two cells of Fig. 9 are typically operated in the Bragg regime with, for example, cell 1 being rotated clockwise and cell 2 being rotated counterclockwise through the Bragg angle. Under these circumstances, the conjugated terms of (45) and (46) are suppressed, and the product transmittance has the form

$$t_{\text{prod}}(x,t) = [1 + j(\tfrac{1}{2})\tilde{v}_1(t - x/V)]\,[1 + j(\tfrac{1}{2})\tilde{v}_2(t + x/V - T)]. \tag{50}$$

If the cell pair is illuminated by a nominally collimated light beam, the pair of openings in the pupil plane mask pass only diffraction components corresponding to the terms $j(\frac{1}{2})\tilde{v}_1(t - x/V)$ and $j(\frac{1}{2})\tilde{v}_2(t + x/V - T)$, with a resultant detector plane intensity distribution given by

$$\begin{aligned} I_d(x,t) &= |j(\tfrac{1}{2})\tilde{v}_1(t - x/V) + j(\tfrac{1}{2})\tilde{v}_2(t + x/V - T)|^2 \\ &= (\tfrac{1}{4})\,|\tilde{v}_1(t - x/V)|^2 + (\tfrac{1}{4})\,|\tilde{v}_2(t + x/V - T)|^2 \\ &\quad + (\tfrac{1}{2})\,\text{Re}\,\{\tilde{v}_1^*(t - x/V)\tilde{v}_2(t + x/V - T)\}. \end{aligned} \tag{51}$$

The detectors in the output plane array perform the integration with respect to time, integrating charge at a rate proportional to the incident light intensity. Thus letting $E_{\Delta T}$ denote the light energy delivered at point x on the detector array during an interval of time T, the output of the integrating detector at x is proportional to

$$\begin{aligned} E_{\Delta T}(x) &= (\tfrac{1}{4})\int_{\Delta T} b_1^2(t - x/V)\, dt + (\tfrac{1}{4})\int_{\Delta T} b_2^2(t + x/V - T)\, dt \\ &\quad + (\tfrac{1}{2})\,\text{Re}\left\{\int_{\Delta T} \tilde{v}_1^*(t - x/V)\tilde{v}_2(t + x/V - T)\, dt\right\}. \end{aligned} \tag{52}$$

To the extent that ΔT can be assumed infinite, the first two terms of this expression evaluate to constants and the third to the desired correlation; thus,

$$E_{\Delta T}(x) = \text{bias} + R_{12}(2x/V - T). \tag{53}$$

In practice, integration times are limited by dark current, which ultimately saturates the linear response of integrating photodetectors. Nevertheless, as suggested earlier, integration times of tens of milliseconds are possible with low noise CCD photodetector arrays, and these times can be extended by post-detection digital integration. The acousto-optic window no longer limits the signal duration, but it does impose a restriction on the correlation variable τ, limiting it to the range $0 \leq \tau \leq W/V$. This restriction can present difficulties in certain

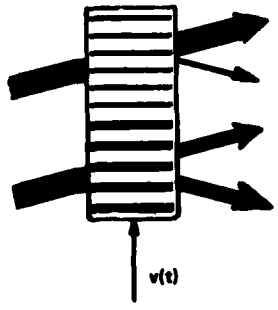

Fig. 10. Zeroth-order depletion.

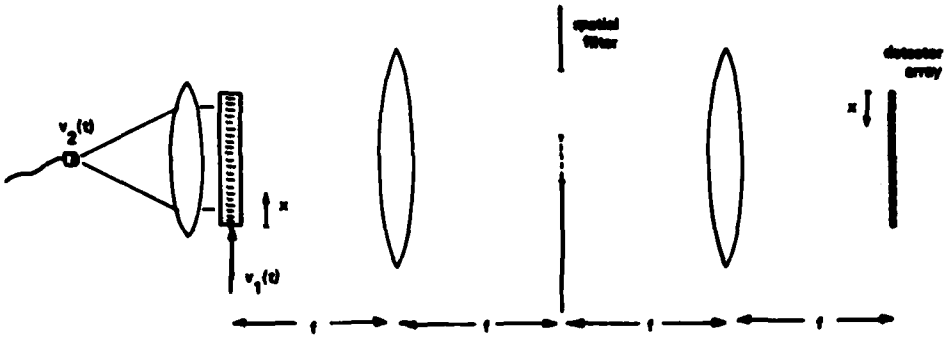

Fig. 11. Single-cell time-integration system. Dotted line in spatial filter denotes phase shifter.

areas of application when, for example, relative time delays between signals are unknown. Perhaps the major limitation of time-integration processors is the presence of the bias terms that attend the desired correlation function. These terms also drive the integrating detectors toward saturation and, because they are signal dependent (both as functions of time and of space), may be difficult to compensate with post-detection processing. In spite of these bias terms, however, excellent processing gain is achievable with time-integration methods when applied to matched filtering operations [27].

A possible drawback of the two-cell system just discussed relates to a phenomenon known as zeroth-order depletion. The basic idea is illustrated graphically in Fig. 10, which shows a bandpass acoustic wave diffracting light in the Bragg regime. Where the acoustic wave is weak, low-efficiency diffraction of the incident beam has relatively little effect on the intensity of the undiffracted component of the output. With high diffraction efficiency, however, a sufficiently large fraction of the incident wave is diffracted that the zeroth order—that part of the wave field that is to be diffracted by the second cell—is modulated both temporally and spatially rather than being constant. High diffraction efficiency operation results in reduced accuracy because of this phenomenon.

C. One-Cell System

Fig. 11 shows an alternate time-integration correlator, of a type described by Turpin [34] and by Kellman [35], that overcomes the zeroth-order depletion limitations of the two-cell system and is generally simpler to implement. The acousto-optic cell, illuminated with light from an LED or laser diode, is driven from the top by signal $v_1(t)$ and imaged onto the integrating detector array. The spatial filter plane mask shifts the phase of the zeroth order by 90° and blocks the frequency-downshifted diffraction component. The intensity of the illumination is modulated by signal $v_2(t)$, such that

$$I_{\text{illum}}(t) = B + v_2(t), \tag{54}$$

where B is a bias sufficiently large to keep the sum $[B + v_2(t)]$ nonnegative. The detector plane intensity is thus given by

$$\begin{aligned} I_d(x,t) &= I_{\text{illum}}(t)\left|1 + (\tfrac{1}{2})\tilde{v}_1(t - x/V)\right|^2 \\ &= [B + v_2(t)]\,[1 + (\tfrac{1}{4})b_1^2(t - x/V) + v_1(t - x/V)] \end{aligned} \tag{55}$$

with associated time-integrated intensity

$$\begin{aligned} E_{\Delta T}(x) = B\Delta T + \int_{\Delta T} &\{Bv_1(t - x/V) \\ &+ v_2(t)[1 + (\tfrac{1}{4})b_1^2(t - x/V)\}\,dt \\ &+ \int_{\Delta T} v_1(t - x/V)v_2(t)\,dt. \end{aligned} \tag{56}$$

The first term in this expression is a spatially uniform bias, which builds up with the integration time ΔT; the second term, being governed by an integrand at the carrier frequency ν_0, is negligable for $\Delta T \gg 1/\nu_0$. The third term, for ΔT sufficiently large, is the desired correlation $R_{12}(\cdot)$ as a function of x/V.

D. One-Cell System with Electronically Inserted Reference

We note briefly a method suggested by Kellman for increasing the versatility and convenience of time-integration acousto-optic processors. The system employed is a simple modification of that of Fig. 11, in which input signal $v_1(t)$ is replaced by signal

$$v_1'(t) = b_1(t)\cos[2\pi(\nu_0 + \nu_c)t + \beta_1(t)] + A\cos 2\pi\nu_0 t \tag{57}$$

obtained from $v_1(t)$ by shifting the carrier frequency by an amount ν_c and adding a cosine signal at that same frequency.

With $v_1'(t)$ as the input, the acousto-optic cell transmittance, assuming Bragg regime operation, is given by

$$t(x, t) = 1 + j[A + (\tfrac{1}{2})\tilde{v}_1(t - x/V)] \exp[j2\pi\nu_c(t - x/V)]. \quad (58)$$

The cell is illuminated as before by the modulated diode and imaged, this time with a zeroth-order stop. The resultant detector plane intensity is given by

$$I_d(x, t) = [B + v_2(t)]\left|A + (\tfrac{1}{2})\tilde{v}_1(t - x/V)\right|^2$$
$$= [B + v_2(t)][A^2 + (\tfrac{1}{4})b_1^2(t - x/V) + Av_1(t - x/V)]. \quad (59)$$

Assuming $\Delta T \gg 1/\nu_0$, the associated time-integrated intensity is approximated by

$$E_{\Delta T}(x) = A^2 B\Delta T + A\int_{\Delta T} v_1(t - x/V)v_2(t)\,dt \quad (60)$$

which is similar to the results for the previous system (which corresponds to setting A equal to unity), but now the ratio of the correlation term to the bias term is proportional to A^{-1} and can therefore be adjusted for optimum system performance [40].

E. Linear Intensity Modulation Method

As our final example, we describe a time-integration correlator/convolver that represents a significant departure from the other systems—both time-integrating and space-integrating—that we have considered to this point. The scheme, described by Sprague and Koliopoulos [33], relies on characteristics of acousto-optic cells operating in the Bragg regime at high diffraction efficiencies. For an acousto-optic modulator with sinusoidal driving signal $v(t) = b\cos 2\pi\nu_0 t$, the intensity of the diffracted wave I_{diff} for Bragg regime operation is given by $I_{\text{diff}} = I_{\text{illum}}\sin^2(Kb)$, where I_{illum} is the intensity of the incident light and K is a constant. For low diffraction efficiency, $Kb \ll 1$ and I_{diff} is approximately equal to $(Kb)^2$, consistent with our earlier analyses. In Sprague's scheme, the driving signal is of the form $v(t) = [b_0 + b_1(t)]\cos 2\pi\nu_0 t$, where b_0 is chosen so as to place operation in the linear portion of the $\sin^2$ curve; i.e., $Kb_0 = \pi/4$. Under these circumstances, the diffracted wave, modulated both temporally and spatially, has the form

$$I_{\text{diff}}(x, t) = I_{\text{illum}}\sin^2[K(b_0 + b_1(t - x/V))]$$
$$= I_{\text{illum}}[(\tfrac{1}{2}) + Kb_1(t - x/V)]. \quad (61)$$

The illuminating beam is modulated according to

$$I_{\text{illum}}(t) = B + b_2(t) \quad (62)$$

and the acousto-optic cell is imaged onto the detector plane with only the diffracted component passed. The resultant detector plane distribution is thus

$$I_d(x, t) = [B + b_2(t)][(\tfrac{1}{2}) + Kb_1(t - x/V)] \quad (63)$$

with integrated intensity

$$E_{\Delta T}(x) = (\tfrac{1}{2})B\Delta T + \int_{\Delta T}[(\tfrac{1}{2})b_2(t) + KBb_1(t - x/V)]\,dt$$
$$+ K\int_{\Delta T} b_1(t - x/V)b_2(t)\,dt \quad (64)$$

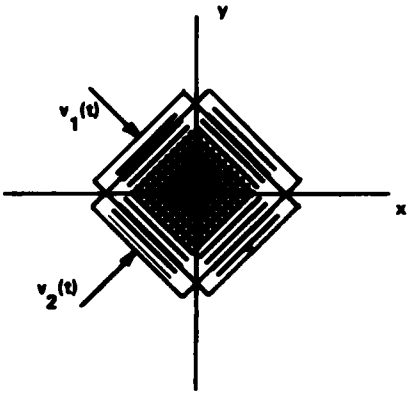

Fig. 12. Cross-ambiguity processor: Input cell geometry.

which consists again of a bias plus the desired correlation term. Because $Kb_1(t)$ is small, the signal-to-bias ratio of the output distribution is itself relatively low.

V. Extensions to Two Dimensions

Although the great majority of acousto-optic processors have 1-D inputs and 1-D outputs, certain 2-D processing operations are possible. The classic example of 2-D acousto-optic processing involves the use of astigmatic imaging systems to allow multiple 1-D correlations or convolutions to be performed in parallel in a channelized system [3]. Systems employed are straightforward extensions of the space-integrating systems discussed in Section III, but the image of the 1-D acousto-optic cell signal $s(x - Vt)$ is spread out in the y-direction to illuminate a mask transparency that varies not only with x but also with y. The single output plane mask and detector become multiple masks and detectors at different distances above the x-axis.

A reasonably sophisticated 2-D acousto-optic processing operation on a *pair* of 1-D signals is the evaluation of the cross-ambiguity function. Given two analytic signals $\tilde{v}_1(t)$ and $\tilde{v}_2(t)$, their cross-ambiguity function is given by

$$\gamma_{12}(\tau, \nu) = \int \tilde{v}_1^*(t - \tau)\tilde{v}_2(t)\exp[j2\pi\nu t]\,dt \quad (65)$$

which can be viewed as the complex correlation of $\tilde{v}_1(t)$ with a frequency-shifted version of $\tilde{v}_2(t)$. A space-integration acousto-optic implementation, described by Said and Cooper [42], is explained with the help of Fig. 12. The two real bandpass signals $v_1(t)$ and $v_2(t)$ are input to a pair of crossed cells, with propagation directions at 45° to the x-y axes. The complex amplitude transmission of the acousto-optic cell pair is given by (ignoring the effect of the window)

$$t_{\text{pair}}(x, y, t) = [1 + js_1(\sqrt{2}[x + y - Vt])]$$
$$\cdot [1 + js_2(\sqrt{2}[x - y - Vt])]. \quad (66)$$

The cell pair is illuminated with a nominally collimated light beam and imaged, with all but one (doubly) diffracted wave component being stopped by a spatial filter plane mask. The transmitted component has the form

$$u_{\text{trans}}(x, y, t) = \tilde{s}_1^*(\sqrt{2}[x + y - Vt])\tilde{s}_2(\sqrt{2}[x - y - Vt]). \quad (67)$$

To pass this component, the spatial filter must consist of an

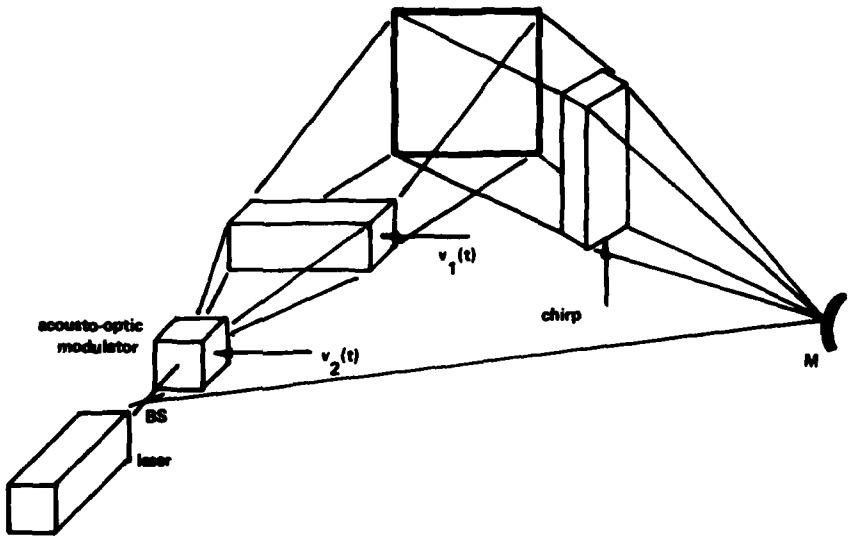

Fig. 13. Time-integration cross-ambiguity processor schematic.

opaque mask with an opening shifted vertically off axis. The wave distribution $u_{trans}(x, y, t)$ is now acted on by an astigmatic lens system that images in the vertical direction while Fourier transforming in the horizontal direction [3]. The resultant output wave amplitude is given by

$$u_{out}(u, y, t) = \int \tilde{s}_1^*(\sqrt{2}[x + y - Vt])\tilde{s}_2(\sqrt{2}[x - y - Vt]) \cdot \exp[j2\pi ux]\, dx \quad (68)$$

which equals $\gamma_{12}(2\sqrt{2}\, y, u)$, as long as both signals are within the aperture. The observed intensity is the squared modulus of this distribution; if phase is to be preserved, interferometric means can be used.

An area of considerable current interest is the application of time integration acousto-optic techniques to 2-D signal processing applications [34], [37], [39]. We illustrate with a system described by Turpin [34] for cross-ambiguity function calculation. Fig. 13 is a schematic representation of this system, greatly simplified to illustrate the concept, not the optics. (The actual system is too complicated optically to illustrate easily, requiring a combination of spherical and cylindrical lenses as well as spatial filtering masks to remove unwanted diffraction components.) Light from the laser source, split by a beamsplitter, travels through two subsystems to be recombined interferometrically in the output plane. In the upper subsystem, the laser beam is first modulated in complex amplitude by an acousto-optic modulator, which is driven by narrow-band signal $v_2(t)$. The output of the acousto-optic modulator is a light beam (a single diffraction component from the cell) with complex amplitude $\tilde{v}_2(t)$. This beam is expanded in the horizontal, or x direction and recollimated so as to illuminate the entire width of the second acousto-optic cell. The output of this second cell, which is driven by signal $v_1(t)$, is expanded and recollimated in the vertical direction and imaged with appropriate spatial filtering in the horizontal direction. The result in the output plane is a complex wave amplitude distribution given by $\tilde{v}_1^*(t - x/V)\tilde{v}_2(t)$. Note that as a function of output plane coordinates this distribution varies only in the x direction.

Also incident on the output plane is the light wave produced by the second subsystem. This wave is planar and is incident at an angle that varies linearly with time in the y direction and is constant in the x direction. Such a wave, described analytically by $\exp[-j2\pi\alpha yt]\exp[-j2\pi\beta x]$, where α and β are constants, can be produced by driving the third acousto-optic cell with a sinusoid that is ramped linearly in frequency—a chirp.

The interference of the waves from the two subsystems produces the intensity distribution

$$\begin{aligned} I_d(x, y, t) &= \left|\tilde{v}_1^*(t - x/V)\tilde{v}_2(t) + \exp(-j2\pi\alpha yt) \cdot \exp(-j2\pi\beta x)\right|^2 \\ &= \left|\tilde{v}_1^*(t - x/V)\tilde{v}_2(t)\right|^2 + 1 \\ &\quad + 2\,\mathrm{Re}\{\exp(j2\pi\alpha x)\tilde{v}_1^*(t - x/V)\tilde{v}_2(t) \cdot \exp(j2\pi\beta yt)\}. \end{aligned} \quad (69)$$

If this distribution is integrated with respect to time, the third term yields

$$2\,\mathrm{Re}\{\exp(j2\pi\alpha x)\tilde{v}_1^*(t - x/V)\tilde{v}_2(t)\exp(j2\pi\beta yt)\}.$$

Assuming that the constant α is sufficiently large, this distribution takes the form of a sinusoidal fringe pattern whose magnitude and phase carry the magnitude and phase of the cross-ambiguity function. Specifically, assuming ΔT to be large, the integrated output intensity is given by

$$E_{\Delta T}(x, y) = \text{bias} + 2|\gamma_{12}(x/V, y)| \cdot \cos[2\pi\alpha x + \arg\{\gamma_{12}(x/V, y)\}]. \quad (70)$$

It should be noted that the accompanying bias distribution is a function of spatial variable x. However, this distribution is spatially low pass in nature. If the output distribution is scanned with a television camera (the camera itself performing the time integration), the output video signal will contain a low-pass component, which can be filtered out, and a bandpass component, which conveys the desired ambiguity function. The tilting plane wave from the lower subsystem must be "restarted" periodically. Assuming it switches back to its starting angle instantaneously, there are certain values of y for which the optical phase of the wave changes continuously with time. For other values of y, however, the phase function $\exp[-j2\pi\beta yt]$ has periodic discontinuities as a function of time.

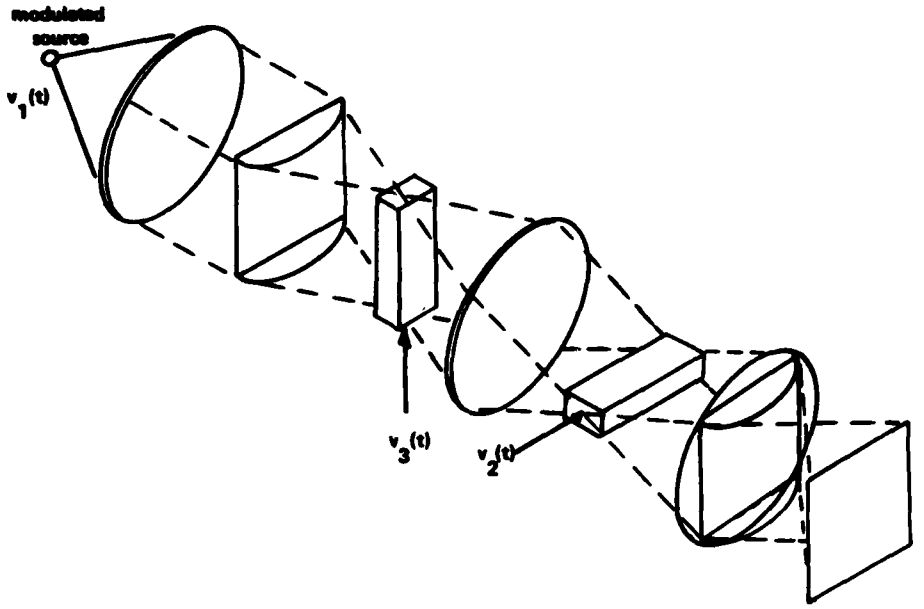

Fig. 14. 2-D triple product time-integration processor. Spatial filtering masks not shown.

Only for those values of y for which the wave phase changes continuously as a function of time is the desired ambiguity function produced. In essence the periodic tilts of the plane wave introduce a comb filter effect in the signal analysis. The total number of discrete frequencies represented by the comb can be shown to equal the time–bandwidth product of the third acousto-optic cell.

The scheme just described is complicated somewhat by the interferometer nature of the system. Not only must a laser be used as the light source, but system construction must be interferometrically stable. Kellman has investigated a class of 2-D time-integration processors based on a simpler, imaging-type architecture [40]. Fig. 14 shows the basic form of such systems. In essence, the two acousto-optic cells of the system are imaged onto each other and onto the output plane, which contains a 2-D array of integrating photodetectors. Intermediate spatial filtering, not shown in the figure for simplicity, leads to a term in the output plane intensity distribution that is given by

$$I(x, y, t) = v_1(t)v_2(t - x/V)v_3(t - y/V). \quad (71)$$

The integrated intensity, as a function of x and y, is thus given by

$$E_T(x, y) = \text{bias} + \int_{\Delta T} v_1(t)\, v_2(t - x/V)v_3(t - y/V)\, dt. \quad (72)$$

Depending on the form of $v_1(t)$, $v_2(t)$, and $v_3(t)$, this system, refered to as a *triple product processor*, can be used for cross-ambiguity calculation or for large time–bandwidth product spectrum analysis (see [18]).

We close this section with a description of a 2-D image processing technique currently under investigation by the author [43] that can be performed using acousto-optic devices. The operation of the overall system is shown schematically in Fig. 15: $f(x, y)$ represents the input image and $h(x, y)$ the spatial impulse response; the output $g(x, y)$ is given by the

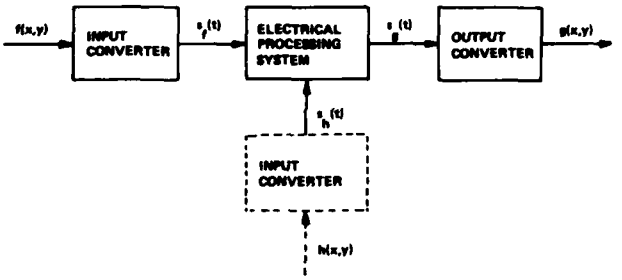

Fig. 15. Image processing system.

2-D convolution $g(x, y) = f(x, y) * h(x, y)$. An essential feature of the system operation is the conversion (invertible through sampling relationships) from 2-D to 1-D signal representations and back again. The acousto-optic system employed for input and output conversion serves the purpose of producing a set of sinusoidal fringes. These fringes, with intensity $I_f(x, y; t) = 1 + \cos[\omega_0 t + 2\pi(ux + vy)]$, result from the interference of light from a pair of mutually coherent light spots. These light spots are scanned in orthogonal directions by acousto-optic beam deflectors to produce fringes of controllable spatial frequency. Depending on the relative temporal frequencies of the two spots (also determined acousto-optically) the fringes may be stationary ($\omega_0 = 0$) or moving with constant phase velocity ($\omega_0 \neq 0$).

Consider the input conversion operation first. We assume that the image to be processed $f(x, y)$ exists as the intensity transmittance of a photo transparency. (It is significant that $f(x, y)$ is the *intensity* transmittance, as opposed to the complex wave amplitude transmittance, of the transparency, for this means that the system is insensitive to such things as emulsion thickness variations and the severely limited dynamic range of wave amplitude spatial light modulators.) This photo-transparency is transilluminated by the fringes and the transmitted light collected by a large photodetector. The detector

output is given by

$$s_d(t) = \int f(x, y) I_f(x, y; t)\, dx\, dy. \tag{73}$$

This signal consists of a dc bias plus an ac term, at frequency ω_0, given by

$$s_f(t) = |F(u, v)| \cos [\omega_0 t + \arg \{F(u, v)\}]$$
$$= \text{Re} \{\exp(-j\omega_0 t) F(u, v)\} \tag{74}$$

where $F(u, v)$ denotes the 2-D Fourier transform of $f(x, y)$. As u and v are varied by changing the inputs to the acousto-optic beam deflectors, $s_f(t)$ conveys sequentially on a temporal carrier the magnitude and phase of the spatial transform of $f(x, y)$. In practice, u and v are scanned in a raster or spiral scan so as to effectively sample the entire transform $F(u, v)$. Scanning is sufficiently slow that $s_f(t)$ is a narrow-band signal.

The electrical signal waveform $s_h(t)$ can be generated in the same way or it can be stored. In any case, we assume it to have the form

$$s_h(t) = |H(u, v)| \cos [\omega_0 t + \arg \{H(u, v)\}] \tag{75}$$

where u and v are again scanned with time ($u = u(t)$, $v = v(t)$) and where $H(u, v)$ is the 2-D Fourier transform of impulse response $h(x, y)$.

The electrical processing system of Fig. 15 consists of an analog multiplier followed by a bandpass filter tuned to the double frequency $2\omega_0$. The output of the filter thus has the form

$$s_g(t) = |G(u, v)| \cos [2\omega_0 t + \arg \{G(u, v)\}] \tag{76}$$

where

$$G(u, v) = F(u, v) H(u, v) \tag{77}$$

i.e., $s_g(t)$ conveys the magnitude and phase of the product of the transforms of $f(x, y)$ and $h(x, y)$ and, therefore, corresponds to the time-signal representation of the desired output $g(x, y)$.

In order to produce output intensity distribution $g(x, y)$ from signal waveform $s_g(t)$, a second, synchronized acousto-optic system is used to produce a fringe pattern of the form

$$I_g(x, y, t) = |G(u, v)| \{1 + \cos [2\pi(ux + vy) + \arg \{G(u, v)\}]\} \tag{78}$$

where u and v are implicit functions of time. Noting that an integration with respect to time corresponds to an integration with respect to u and v, the time-integrated intensity distribution $\int I_g(x, y)\, dt$ is easily shown to equal a bias plus the (real) distribution $g(x, y)$. Contrast is low, but computer simulations have shown it to be adequate for many applications.

VI. Concluding Remarks

This paper has surveyed the major techniques developed to date for effecting signal convolutions and correlations with acousto-optic devices. The emphasis has been on a Fourier optics point of view; distinctions between different possible modes of operation—Bragg regime, Raman–Nath regime, linear in wave amplitude, linear in wave intensity, phase preserving, etc.—have received major emphasis in hopes of avoiding possible confusion. Although the treatment is by no means exhaustive, it should serve as an adequate basis for an understanding of most of the literature in this field.

The support of the U.S. Air Force Office of Scientific Research for much of the author's research in acousto-optic signal processing is gratefully acknowledged.

References

[1] F. Okolicsany, "The wave-slot, an optical television system," *Wireless Eng.*, vol. 14, pp. 527–536, Oct. 1937.
[2] F. Vilbig, "An apparatus for speech compression and expansion and for replaying visible speech records," *J. Acoust. Soc. Amer.*, vol. 22, pp. 754–761, Nov. 1950.
[3] L. J. Cutrona, E. N. Leith, C. J. Palermo, and L. J. Porcello, "Optical data processing and filtering systems," *IRE Trans. Inform. Theory*, vol. IT-6, pp. 386–400, June 1960.
[4] A. H. Rosenthal, "Application of ultrasonic light moduation to signal recording, display, analysis, and communication," *IRE Trans. Ultrasonics Eng.*, vol. UE-8, pp. 1–5, Jan. 1961.
[5] L. Slobodin, "Optical correlation technique," *Proc. IEEE*, vol. 51, p. 1782, Dec. 1963.
[6] M. Arm, L. Lambert, and I. Weissman, "Optical correlation technique for radar pulse compression," *Proc. IEEE*, vol. 52, p. 842, July 1964.
[7] J. S. Gerig and H. Montague, "A simple optical filter for chirp radar," *Proc. IEEE*, vol. 52, p. 1753, Dec. 1964.
[8] D. H. McMahon, "Pulse compression via Brillouin scattering in the Bragg limit," *Proc. IEEE*, vol. 55, pp. 1602–1612, Sept. 1967.
[9] M. B. Schulz, M. G. Holland, and L. Davis, Jr., "Optical pulse compression using Bragg scattering by ultrasonic waves," *Appl. Phys. Lett.*, vol. 11, pp. 237–240, Oct. 1967.
[10] J. H. Collins, E. G. H. Lean, and H. J. Shaw, "Pulse compression by Bragg diffraction of light with microwave sound," *Appl. Phys. Lett.*, vol. 11, pp. 240–242, Oct. 1967.
[11] M. King, W. R. Bennett, L. B. Lambert, and M. Arm, "Real-time electrooptical signal processors with coherent detection," *Appl. Opt.*, vol. 6, pp. 1367–1375, Aug. 1967.
[12] E. B. Felstead, "A simple real-time incoherent optical correlator," *IEEE Trans. Aerosp. Electron. Syst.*, vol. AES-3, pp. 907–914, Nov. 1967.
[13] R. W. Dixon, "Acoustic diffraction of light in anisotropic media," *IEEE J. Quantum Electron.*, vol. QE-3, pp. 85–93, Feb. 1967.
[14] G. Meltz and W. T. Maloney, "Optical correlation of Fresnel images," *Appl. Opt.*, vol. 7, pp. 2091–2099, Oct. 1968.
[15] R. Whitman, A. Korpel, and S. Lotsoff, "Applications of acoustic Bragg diffraction to optical processing techniques," in *Modern Optics (Proc. Symp. Modern Optics*, Microwave Res. Inst. Symposia Series, vol. XVII), Brooklyn, NY: Polytechnic Press, 1967, pp. 243–256.
[16] H. R. Carleton, W. T. Maloney, and G. Meltz, "Colinear heterodyning in optical processors," *Proc. IEEE*, vol. 57, pp. 769–775, May 1969.
[17] W. T. Maloney, "Acoustooptical approaches to radar signal processing," *IEEE Spectrum*, vol. 6, pp. 40–48, Oct. 1969.
[18] T. Turpin, "Spectrum analysis using optical processing" this issue, pp. 79–92.
[19] J. W. Goodman, *Introduction to Fourier Optics.* New York: McGraw-Hill, 1968.
[20] A. Papoulis, *Systems and Transforms with Applications in Optics.* New York: McGraw-Hill, 1968.
[21] A. Vander Lugt, "Coherent optical processing," *Proc. IEEE*, vol. 62, 1300–1319, Oct. 1974.
[22] I. C. Chang, "Acoustooptic devices and applications," *IEEE Trans. Sonics Ultrasonics*, vol. SU-23, pp. 2–22, Jan. 1976.
[23] D. L. Hecht, "Multifrequency acousto-optic diffraction," *IEEE Trans. Sonics and Ultrasonics*, vol. SU-24, pp. 7–18, Jan. 1977.
[24] M. I. Skolnik, *Radar Handbook.* New York: McGraw-Hill, 1970, ch. 3.
[25] A. Korpel, "Acousto-optics—A review of fundamentals," this issue, pp. 48–53.
[26] R. W. Damon, W. T. Maloney, and D. H. McMahon, "Interaction of light with ultrasound: phenomena and applications," in *Physical Acoustics*, W. P. Mason and R. N. Thurston, Eds., vol. 7, New York: Academic Press, 1970, pp. 273–366.
[27] R. A. Sprague, "A review of acousto-optic signal correlators," *Opt. Eng.*, vol. 16, pp. 467–474, Sept./Oct. 1977.
[28] N. J. Berg, J. N. Lee, M. W. Casseday, and B. J. Udelson, "Surface wave delay line acoustooptic devices for signal processing," *Appl. Opt.*, vol. 18, pp. 2767–2774, 1979.
[29] A. Korpel, "Acoustooptic signal processing," in *Optical Information Processing*, Yu. E. Nesterikhin, G. W. Stroke, and W. E. Kock, Eds. New York: Plenum, 1976, pp. 171–193.
[30] J. M. Florence and W. T. Rhodes, "Frequency-variant signal processing using a channelized optical system," submitted to *Opt. Lett.*

[31] M. Gottlieb, J. J. Conroy, and T. Foster, "Optoacoustic processing of large time-bandwidth signals," *Appl. Opt.*, vol. 11, pp. 1068–1077, May 1972.
[32] R. M. Montgomery, "Acousto-optical signal processing system," U.S. Patent 3 634 749, Jan. 1972.
[33] R. A. Sprague and C. L. Koliopoulos, "Time integrating acousto-optic correlator," *Appl. Opt.*, vol. 15, pp. 89–92, Jan. 1976.
[34] T. M. Turpin, "Time integrating optical processors," in *Real-Time Signal Processing*, F. Tao, Ed. (*Proc. SPIE*, vol. 154, 1978), pp. 196–203, 1978.
[35] P. Kellman, "Detector integration acousto-optic signal processing," in *Proc. 1978 Int. Optical Comp. Conf.* (*Digest of Papers*), (IEEE No. 78CH-1305-2C), pp. 91–95, 1978.
[36] ——, "Time integrating optical processors," in *Optical Processing Systems*, W. Rhodes, Ed. (*Proc. SPIE*, vol. 185, 1979), pp. 130–139, 1979.
[37] ——, "Time integrating optical signal processing," in *Acousto-Optic Bulk Wave Devices*, J. Houston, Ed. (*Proc. SPIE*, vol. 214, 1979), pp. 63–73, 1979.
[38] T. R. Bader, "Acoustooptic spectrum analysis: a high performance hybrid technique," *Appl. Opt.*, vol. 18, pp. 1668–1672, May 1979.
[39] J. D. Cohen, "Ambiguity processor architectures using one-dimensional acousto-optic transducers," in *Real-Time Signal Processing II*, T. F. Tao, Ed. (*Proc. SPIE*, vol. 180, 1979), pp. 134–142, 1979.
[40] P. Kellman, "Time integrating optical signal processing," Ph.D. dissertation, Stanford University, Stanford, CA, June 1979.
[41] P. S. Guilfoyle, D. L. Hecht, and D. L. Steinmetz, "Joint transform time-integrating acousto-optic correlator for chirp spectrum analysis," in *Active Optical Devices*, J. Tracy, Ed. (*Proc. SPIE*, vol. 202, 1979), pp. 154–162, 1979.
[42] R. A. K. Said and D. C. Cooper, "Crosspath real-time optical correlator and ambiguity function processor," *Proc. Inst. Elec. Eng.*, vol. 120, pp. 423–428, Apr. 1973.
[43] W. T. Rhodes, "Acousto-optic devices applied to image processing," in *Real-Time Signal Processing*, F. Tao, Ed. (*Proc. SPIE*, vol. 180, 1979), pp. 143–149, 1979.

III. THE FALLING RASTER IN TIME-INTEGRATION FOLDED SPECTRUM ANALYSIS

[An excerpt from "The Falling Raster in Optical Signal Processing," to be published in Transformations in Optical Signal Processing, W. Rhodes, J. Fienup, and B. Saleh, eds. (SPIE, Bellingham, 1982; Volume 2 in Advanced Institute Series).]

In optical processing we usually associate the falling raster with space-integration folded spectrum analysis. However, it also plays a critical role in the folded spectrum analysis of 1-D signals using time-integration optical processing methods [11-18]. In this section we consider this aspect of the falling raster, starting with what we have found to be an extremely useful analogy between time-integration optical spectrum analysis and incoherent holography.

A. Incoherent Holography Analogy

In Fig. 9a we show a conventional coherent optical spectrum analyzer with falling raster input and folded spectrum output. Consider now the situation shown in Fig. 9b, where the raster recording, rather than being uniformly illuminated, is scanned, line by line. Clearly a folded spectrum cannot result from such an operation, since at any time wave intensity in the back focal plane of the lens is uniform. If, however, as shown in Fig. 9c, a *reference wave, mutually coherent with the scan wave,* is introduced by focusing a spot off axis in the raster plane, the output-plane intensity will at any time consist of a sinusoidal fringe pattern. If photographic film in that plane integrates the incident intensity pattern as the raster is scanned, the result is, in most aspects, equivalent to a Fourier transform hologram of the raster record. Specifically, each sample value along the raster (and, therefore, each sample in time of the waveform f(t)) is mapped into a sinusoidal fringe pattern whose amplitude (and, if the raster is complex-valued, phase) is determined by the (complex) amplitude of the sample. So long as the focused reference point is sufficiently far off axis, each such fringe pattern is characterized by a unique spatial frequency.

In Fig. 9d, the situation is similar, except that now the raster record has been removed and the scanning beam is modulated, e.g., by an electro-optic modulator, as it scans. So long as the scanning beam is modulated in time in the same way as it would by transmission through the raster recording itself, the result in the output plane is the same time-integrated fringe pattern as for Fig. 9c. Note that an identical time-integration pattern will result if it is the scanned light spot that has the constant amplitude and the non-scanned spot that varies as f(t). Indeed, one beam can vary in amplitude as a(t) and the other as b(t), again with the same result, so long as $a(t)b^*(t) = f(t)$.

The system of Fig. 9d contains all the essential features of an interferometric 2-D time-integration spectrum analyzer for 1-D signals: a scanner executing a falling raster, a modulator, a

reference source, and a time-integrating detector to record or otherwise measure the integrated fringe pattern that builds up with time in the output plane. In practical systems the detector is a CCD array or a TV-type camera.

The resemblance the output of this system bears to a Fourier-transform hologram of the raster record merits special emphasis. In Fig. 9e a conventional (i.e., no time integration) Fourier-transform hologram recording setup is shown. Both this system and the time integration system of Fig. 9d produce the same bandpass structure in the recorded output. Ignoring unimportant low spatial frequency structure, the time integration system can be said to record a hologram of the folded spectrum associated with the raster signal. Since the hologram is of the off-axis reference kind, both magnitude and phase of the folded spectrum are preserved.

At the same time, there is an extremely important difference between the conventional space-integration Fourier transform hologram of Fig. 9e and the time-integration pattern of Fig. 9d: bias. With space integration, all points on the raster are illuminated simultaneously, and a relatively high contrast hologram can result. With time integration, on the other hand, each fringe pattern is produced separately, and each carries its own bias. This latter situation is directly analogous to incoherent holography, where only low contrast holograms result when objects of large space-bandwidth product are recorded via incoherent holography [19]. This bias problem is severe. However, as we discuss elsewhere [20], significant improvements in signal-to-bias ratio are possible if the time-integration recording system is modified to produce fringes that always have unity visibility. Related techniques can be applied to non-interferometric time-integration systems with similar improvement in signal-to-bias ratio.

B. Distributed Local Oscillator Point of View

The holographic point of view presented above differs from that generally taken by other authors. Indeed, there are many different ways of viewing time-integration optical processing, each providing its own particular insight. In his original paper on the subject [11] and in his article in this volume [18], Turpin emphasizes the concept of a spatially distributed local oscillator array. Figure 10 helps clarify the relationship between the holographic and the local oscillator points of view. In that figure, it is the scanned light spot that is constant in amplitude and the non-scanned spot that varies as f(t). Clearly the time-integration fringe pattern that results is the same as that obtained with the system of Fig. 9d. However, rather than being described as a buildup of fringe patterns, the time-integration process is now described in terms of a mixing, in the output plane, of a wave with complex amplitude $f(t)\exp[i2\pi ux]$ with a second wave whose optical frequency varies from point to point: a local oscillator (LO) wave whose frequency is location dependent. As Turpin notes, the space-dependent frequency of this wave can be

viewed as a consequence of a location-dependent Doppler shift: the raster-scanned spot produces in the output plane a plane wave that tilts rapidly left-to-right and slowly top-to-bottom. The progressive tilt of this wave with time produces varying amounts of Doppler shift at different points on the detector surface. Over a small local region of the detector plane where the LO wave has essentially constant Doppler frequency ν_n, the output plane intensity is given by

$$I(u,v,t) = |f(t)\exp[-i2\pi\alpha u] + \exp[i2\pi\nu_n t]|^2$$

$$= 1 + |f(t)|^2$$

$$+ 2\,\mathrm{Re}\{\exp[-i2\pi\alpha u]f(t)\exp[-i2\pi\nu_n t]\}. \qquad (9)$$

If this intensity is integrated with respect to time over period T, the third term yields a spatial sinusoid whose magnitude and phase are governed by the short-time Fourier spectrum of f(t):

$$|F_T(\nu_n)|\cos[2\pi\alpha u + \arg\{F_T(\nu_n)\}] \qquad (10)$$

where

$$F_T(\nu_n) = \int_T f(t)\exp[-i2\pi\nu_n t]dt. \qquad (11)$$

If T exceeds the duration of f(t), output is governed by the conventional Fourier spectrum. By looking at different local regions in the output plane, one can measure the magnitude and phase of the Fourier spectrum over a range of frequencies.

(If the scanning spot in Fig. 10d is scanned acoustooptically, there is an additional complicating quirk: the light spot is <u>itself</u> shifted in frequency as it scans. In this case it is necessary to introduce a compensating shift in the frequency of the interfering (signal) wave. The result is a chirp algorithm implementation of the Fourier transform. See, for example, [13].)

C. <u>Moving Comb Function Model</u>

Specific characteristics of the spatially distributed local oscillator wave can be analyzed through the use once again of a spatial comb function, this time one that is translated with constant velocity. The comb function model also serves to consolidate the distributed local oscillator and falling raster points of view.

Our approach to modeling the raster-scanned light spot is illustrated in Fig. 11. In Fig. 11a we show a linear string of impulses being translated past a stationary window. Since the impulse spacing equals the window width, there is always a single impulse within the window at a given time, and con :ant-velocity translation of the impulse string results in a single falling-raster scan of the window. In Fig. 11b it is a 2-D comb of

impulses that is translated past the window. Again there is only a single impulse in the window at a given time, but translation of the comb results in a repetitive falling raster scan of the window. We choose θ to satisfy the condition

$$\tan\theta = H/NW, \quad N \text{ integer}, \tag{12}$$

in which case the repetitive raster scan is truly periodic--i.e., subsequent scans retrace previous ones exactly, with N lines appearing in the raster.

Analytically we model the single scan of Fig. 11a by

$$f_{SCAN}(x,y;t) = [R_\theta\{(1/W)\,\mathrm{comb}(x/W)\,\delta(y)\} ** \delta(x-Vt,y)] \cdot R_\theta\{\mathrm{rect}(x/W, y/H)\}, \tag{13}$$

where V is the translational velocity in the x-direction. The local oscillator distribution corresponding to this scan is given by the 2-D spatial Fourier transform of $f_{SCAN}(x,y;t)$,

$$F_{SCAN}(u,v;t) = [R_\theta\{\mathrm{comb}(Wu)\,1(v)\}\exp[-i2\pi uVt] ** R_\theta\{WH\,\mathrm{sinc}(Wu,Hv)\}. \tag{14}$$

Ignoring for the moment the sinc-function smoothing, this latter distribution consists of line impulses oriented as in Fig. 6b. Through the factor $\exp[-i2\pi uVt]$ the temporal frequency of the wave amplitude along these lines is shifted in proportion to u. Thus there is a continuous range of local oscillator frequencies present in the distribution. As was true for the space-integration case of Fig 6d, there is a coarse frequency direction (in the u-direction) and a fine frequency direction (along the impulse lines). The separation 1/W between sinc function nulls again equals the line impulse spacing; convolution in the direction perpendicular to the impulse lines thus leads to multiple temporal frequencies between the lines but not on the lines. The amount of convolution blurring in the fine-frequency direction depends on the window length H and, thereby, on the duration of the scan. At any point along one of these lines, there is a spread of frequencies present in the range $\Delta\nu \cong 1/T \cong V/NW$, where T is the total scan time. That is, of course, consistent with the observation that window height determines how long the local oscillator wave is present and thus determines spectral resolution.

The periodic raster scan of Fig. 11b is modeled by

$$g_{scan}(x,y;t) = [R_\theta\{(1/WH)\,comb(x/W,y/H)\} ** \delta(x-Vt,y)]$$

$$\cdot R_\theta\{rect(x/W,y/H)\}, \qquad (16)$$

which has Fourier transform

$$G_{scan}(u,v;t) = [R_\theta\{comb(Wu,Hv)\}\,exp[-i2\pi uVt]]$$

$$** R_\theta\{WH\ sinc(Wu,Hv)\}. \qquad (17)$$

The two terms entering into this convolution are illustrated in Fig. 12. The local oscillator distribution consists of discrete points of light, separated in temporal frequency ty $1/T = V/NW$. These spots are blurred by the sinc function convolution, but in such a way that their discrete-frequency local oscillator character is preserved at the spot centers. Those spots contained within the dashed lines of Fig. 12 span the entire range of frequencies available.

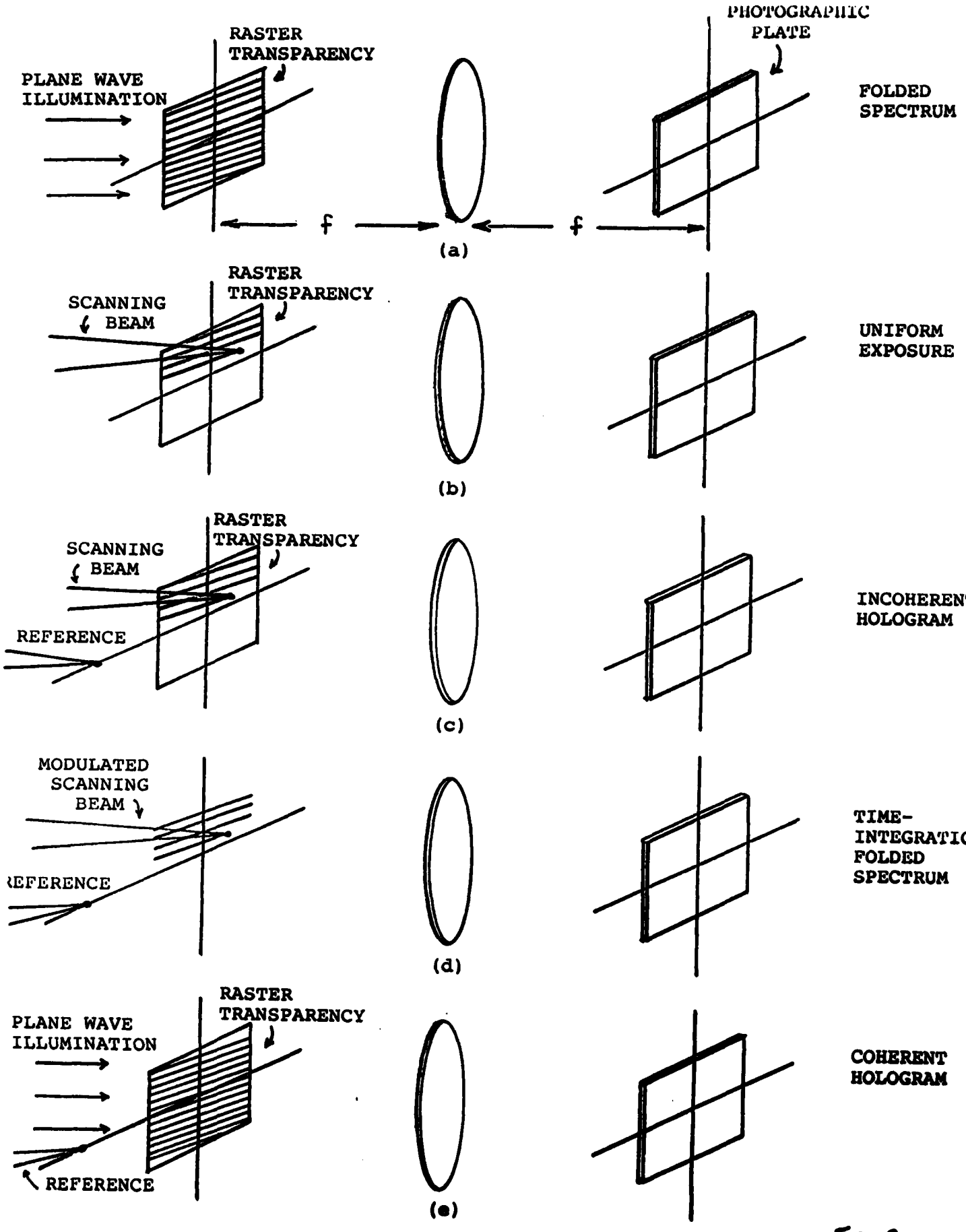
PHOTOGRAPHIC PLATE
RASTER TRANSPARENCY
PLANE WAVE ILLUMINATION
FOLDED SPECTRUM
f
f
(a)
RASTER TRANSPARENCY
SCANNING BEAM
UNIFORM EXPOSURE
(b)
RASTER TRANSPARENCY
SCANNING BEAM
REFERENCE
INCOHERENT HOLOGRAM
(c)
MODULATED SCANNING BEAM
REFERENCE
TIME-INTEGRATION FOLDED SPECTRUM
(d)
RASTER TRANSPARENCY
PLANE WAVE ILLUMINATION
REFERENCE
COHERENT HOLOGRAM
(e)

Fig. 9


MODULATED
NON-SCANNING
BEAM
SCANNING
LOCAL OSCILLATOR
BEAM

Fig. 10

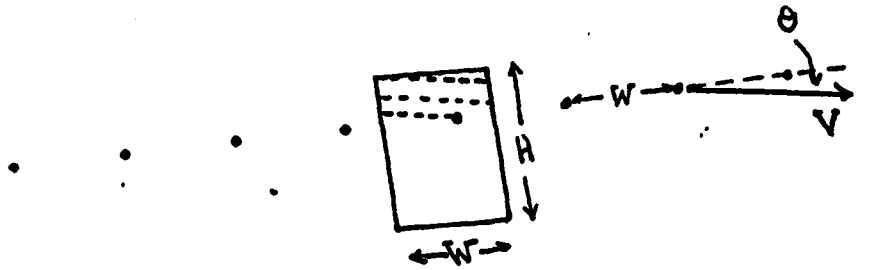

(a)

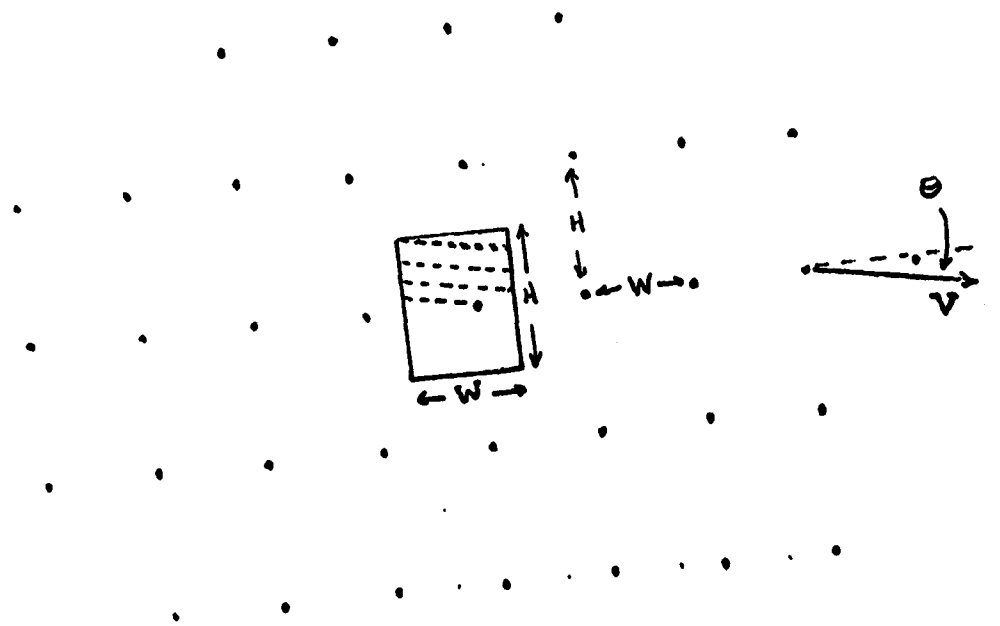

(b)

Fig. 11

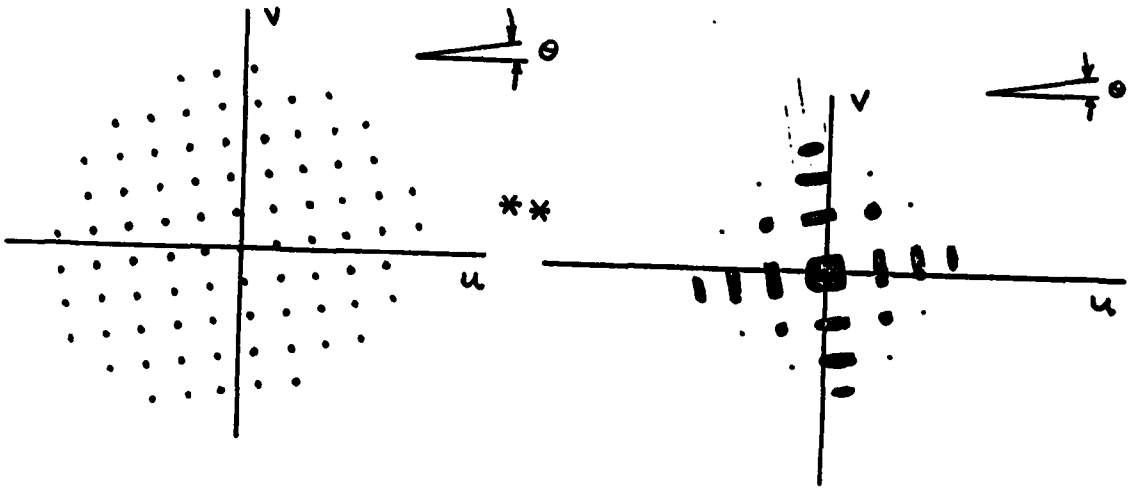

Fig. 12


DAT
ILM